Hindawi Publishing Corporation
Advances in High Energy Physics
Volume 2015, Article ID 612390, 30 pages
http://dx.doi.org/10.1155/2015/612390

Review Article

Charged Particle, Photon Multiplicity, and Transverse Energy Production in High-Energy Heavy-Ion Collisions

Raghunath Sahoo,[1] Aditya Nath Mishra,[1] Nirbhay K. Behera,[2] and Basanta K. Nandi[2]

[1]*Indian Institute of Technology Indore, Indore 452017, India*
[2]*Indian Institute of Technology Bombay, Mumbai 400067, India*

Correspondence should be addressed to Raghunath Sahoo; raghunath.sahoo@cern.ch

Received 24 August 2014; Revised 17 January 2015; Accepted 24 January 2015

Academic Editor: Andrey Leonidov

We review the charged particle and photon multiplicities and transverse energy production in heavy-ion collisions starting from few GeV to TeV energies. The experimental results of pseudorapidity distribution of charged particles and photons at different collision energies and centralities are discussed. We also discuss the hypothesis of limiting fragmentation and expansion dynamics using the Landau hydrodynamics and the underlying physics. Meanwhile, we present the estimation of initial energy density multiplied with formation time as a function of different collision energies and centralities. In the end, the transverse energy per charged particle in connection with the chemical freeze-out criteria is discussed. We invoke various models and phenomenological arguments to interpret and characterize the fireball created in heavy-ion collisions. This review overall provides a scope to understand the heavy-ion collision data and a possible formation of a deconfined phase of partons via the global observables like charged particles, photons, and the transverse energy measurement.

1. Introduction

At extreme temperatures and energy density, hadronic matter undergoes a phase transition to partonic phase called Quark-Gluon Plasma (QGP) [1–3]. The main goal of heavy-ion collision experiments is to study the QGP by creating such extreme conditions by colliding heavy nuclei at relativistic energies. During the last decade, there are many heavy-ion collision experiments carried out at SPS, RHIC, and LHC to create and study QGP in the laboratory. Global observables like transverse energy (E_T), particle multiplicities (N_γ, N_{ch}, etc.), p_T-spectra of the produced particles, and their pseudorapidity distributions ($dE_T/d\eta, dN/d\eta$) with different colliding species and beam energies provide insight about the dynamics of the system and regarding the formation of QGP [2, 4]. It is also proposed that the correlation of mean transverse momentum $\langle p_T \rangle$ and the multiplicity of the produced particles may serve as a probe for the Equation of State (EoS) of hot hadronic matter [5]. In a thermodynamic description of the produced system, the rapidity density (dN/dy) reflects the entropy and the mean transverse momentum ($\langle p_T \rangle$) corresponds to the temperature of the system. Except at the phase transition points, the rapidity density linearly scales with $\langle p_T \rangle$. If the phase transition is of first order, then the temperature remains constant at the coexistence of the hadron gas and the QGP phase, thereby increasing the entropy density. In such a scenario, $\langle p_T \rangle$ shows a plateau with increase of entropy, thereby characterizing the phase transition associated with the time evolution of the system. Hence, the global observables like dN/dy and $\langle p_T \rangle$ give indication of a possible existence of a QGP phase and the order of phase transition. $dE_T/d\eta$ gives the maximum energy density produced in the collision process which is necessary to understand the reaction dynamics. The formation of QGP may also change the shape of the pseudorapidity distribution [6, 7]. The event

multiplicity distribution gives information of the centrality and energy density of the collision. The scaling of multiplicity with number of participant nucleons (N_{part}) reflects the particle production due to soft processes (low-p_T). However, at high energy when hard processes (high-p_T) dominate, it is expected that the multiplicity will scale with the number of nucleon-nucleon collisions (N_{coll}). There are models [8] to explain the particle production taking a linear combination of N_{part} and N_{coll} (called two-component model). The most viable way of studying QGP is via the particles produced in the collision in their respective domain of proposed methods. Then one of the most fundamental questions arises about the mechanism of particle production and how they are related with the initial energy density, gluon density in the first stage of the collision evolution, and entropy of the system. Similarly, question can be put to figure out the role of soft and hard process of particle productions. It is proposed that the charged particle multiplicity technically called the pseudorapidity density distributions of charged particles, $dN_{\text{ch}}/d\eta$, can be used to address the above questions [9–15]. Here the pseudorapidity is defined as, $\eta = -\ln \tan \theta/2$, where θ is the polar angle made by the produced particles with the detector, with respect to the beam direction. So $dN_{\text{ch}}/d\eta$ is called one of the global variables to characterize the system produced in the heavy-ion collisions. Experimentally, it is more easy to estimate this quantity as most of the detectors are capable of detecting charged particles and it involves only kinematics of the charged particles.

In this review, in Section 2, we discuss the method of experimental determination of collision centrality, which is followed by discussions on the midrapidity pseudorapidity density distributions of charged particles for different collision energies, collision species, and centralities in Section 3. In this section, we discuss the longitudinal scaling and factorization of charged particles. The expansion dynamics of the system is discussed using the pseudorapidity density distributions of charged particles and the Landau-Carruthers hydrodynamics. In subsequent subsections, the scaling of total charged particles with collision centrality and its energy dependence are discussed. This is followed with similar discussions on the photon pseudorapidity density at forward rapidities in Section 4, which includes longitudinal scaling of photons. Subsequently, in Section 5, discussions are made on the production of transverse energy and its use for centrality determination. Section 6 includes discussions on collision energy dependence of transverse energy, which is followed by discussions on the centrality dependence in Section 7. Section 8 includes discussions on estimation of initial energy density in Bjorken hydrodynamic scenario and its energy and centrality dependences. Further we correlate the energy and centrality dependence of transverse energy per charged particle with chemical freeze-out criteria in Section 9. In Section 10, we summarize the review with conclusions. Appendix discusses the important properties of Gamma and Negative Binomial Distributions.

2. Centrality Determination

In heavy-ion collisions, the event centrality is of utmost importance to understand the underlying physics of the collision. The event centrality is related to the impact parameter, defined as the distance between the centroids of the two colliding nuclei in a plane transverse to the beam axis, of the collision. The impact parameter tells about the overlap volume of the two nuclei. This overlap volume determines the geometrical parameters, like number of participant nucleons (N_{part}), number of spectator nucleons (N_{spec}), and the number of binary collisions (N_{coll}).

The impact parameter can not be determined experimentally. However, the global observables, like total charged particles (N_{ch}), transverse energy (E_T), or energy deposited in ZDC (E_{zdc}), and so forth, are related to this geometrical quantity. By combining the experimental observables with simulation, one can estimate the impact parameter and hence the centrality of the event class. The centrality is expressed as the percentile (c) of the total hadronic interaction cross section corresponding to the charged particle multiplicity above certain threshold and is given by

$$c = \frac{1}{\sigma_{AA}} \int_0^b \frac{d\sigma}{db'} db'. \tag{1}$$

In (1), σ_{AA} is the total nuclear interaction cross section of $A+A$ collision. Assuming constant luminosity, the cross section can be replaced by the number of observed events after the trigger efficiency correction. But at very high energy, when these two nuclei pass by each other, there is a large QED cross section because of the electromagnetic field [16, 17]. This QED cross section is much larger than the hadronic cross section and this contaminates the most peripheral events. That is why the centrality determination is restricted to some percentile where the QED contribution is negligible. The fraction of hadronic events excluded by such cut as well as the trigger efficiency can be estimated by using a Glauber model simulation.

For a given impact parameter, the N_{part} and N_{coll} can be estimated by Glauber Monte Carlo method. The parametrized Negative Binomial Distribution (NBD) can be used to describe the nucleon-nucleon collisions. For heavy-ion collisions, N_{part} and N_{coll} are used to generate the number of charged particles by incorporating two-component model in the following way:

$$N_{\text{ancestors}} = f \times N_{\text{part}} + (1 - f) \times N_{\text{coll}}. \tag{2}$$

This $N_{\text{ancestors}}$ refers to the "independent emitting source." The two-component model given in (2) incorporates the soft and hard interactions. Soft process is related to the N_{part} and hard process is related to N_{coll}.

The functional form of NBD distribution is given by

$$P(\mu, k, n) = \frac{\Gamma(n + k)}{\Gamma(n + 1)\,\Gamma(k)} \cdot \frac{(\mu/k)^n}{(\mu/k + 1)^{n+k}}. \tag{3}$$

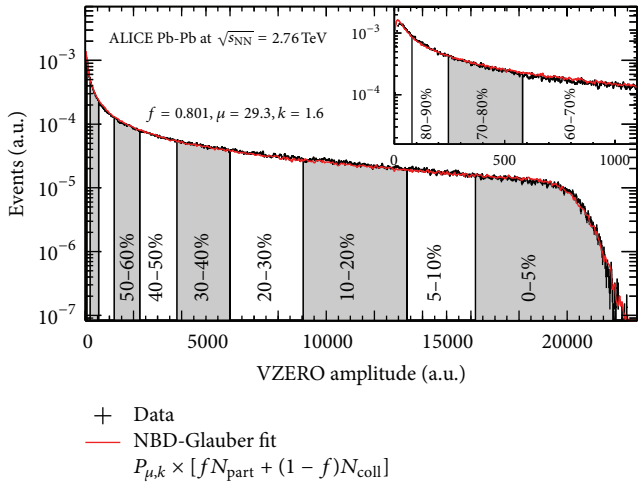

FIGURE 1: Distribution of the summed amplitudes in the VZERO scintillator tiles (histogram); inset shows the low amplitude part of the distribution. The curve shows the result of the Glauber model fit to the measurement. The vertical lines separate the centrality classes used in the analysis, which in total correspond to the most central 80% of hadronic collisions. The figure is taken from [21].

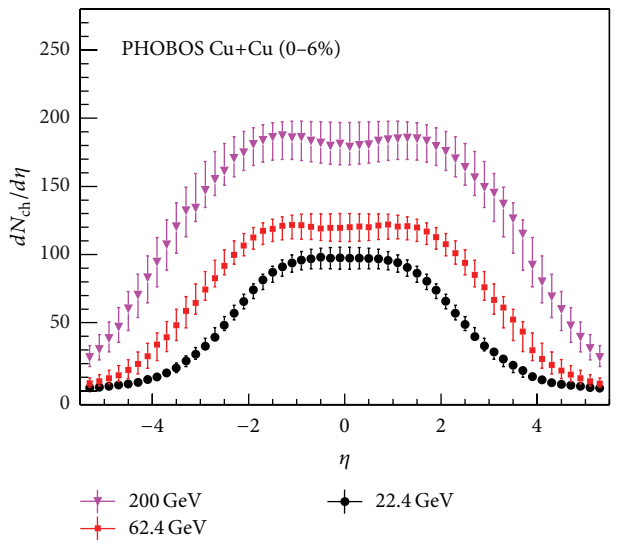

FIGURE 2: Charged particle pseudorapidity distributions of Cu+Cu collision systems for the most central events for different collision energies.

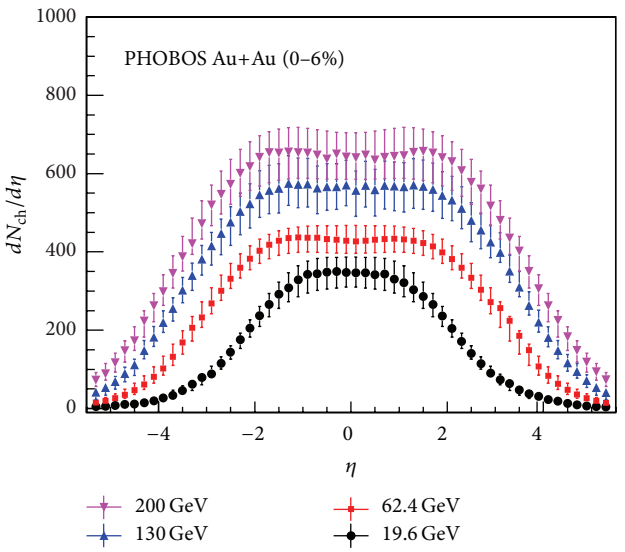

FIGURE 3: Charged particle pseudorapidity distributions of Au+Au collision system for the most central events for different collision energies.

Equation (3) represents the probability of measuring n hits per ancestor. Here, μ represents the mean multiplicity per ancestor and k controls the width of the distribution. In $p + p(\overline{p})$ collision, a Negative Binomial Distribution (NBD) with a fixed value of μ and k well describes the charged multiplicity data for most of multiplicity range though requiring a second NBD ingredient to well describe the tail of the distribution [18–20]. The charged particle multiplicity for nucleus-nucleus collisions with a given impact parameter is generated by sampling $N_{\text{ancestors}}$ times the $p + p$ multiplicity, which is generated by using NBD. Finally, a χ^2 minimisation is done by fitting the Glauber Monte Carlo generated multiplicity and the charged particle multiplicity obtained from the collision data. The χ^2 minimization will give us the value of f, μ, and k. This gives a connection between an experimental observable and a Glauber Monte Carlo. From this one can have access to N_{part} and N_{coll} for a given class of centrality by NBD-Glauber fit. For example, the centrality determination in ALICE using VZERO (V0) amplitude is given in Figure 1. The two-component model is fitted with the V0 amplitude in Figure 1 to find out the N_{part} and N_{coll} values for a corresponding centrality [16].

3. Pseudorapidity Density Distribution of Charged Particles ($dN_{\text{ch}}/d\eta$)

3.1. Energy Dependence of $dN_{ch}/d\eta$ for Different Collision Species. The $dN_{\text{ch}}/d\eta$ distributions as a function of pseudorapidity of most central events for Cu+Cu collisions at $\sqrt{s_{\text{NN}}}$ = 22.4 GeV, 62.4 GeV, and 200 GeV are given in Figure 2 [22]. Similarly, the $dN_{\text{ch}}/d\eta$ distributions for Au+Au system at $\sqrt{s_{\text{NN}}}$ = 19.6 GeV, 62.4 GeV, 130 GeV, and 200 GeV are given in Figure 3 [9, 23]. Both the collision systems, that is, Cu+Cu and Au+Au, data are from PHOBOS experiment which has maximum pseudorapidity coverage of $|\eta| < 5.3$ at RHIC. In Figure 4, the charged particle pseudorapidity distributions of Pb+Pb collisions at different energies are presented. The filled circles and star markers correspond to the fixed target experiment for beam energies 40 AGeV and 158 AGeV, respectively. For the fixed target experiment, the x-axis is $\eta - \eta_{\text{peak}}$. Here, η_{peak} corresponds to the peak position of the $dN_{\text{ch}}/d\eta$ distribution in the fixed target experiment. Theoretically, for fixed target environment, the $\eta_{\text{peak}} = \eta_{\text{mid}} = y_{\text{beam}}/2$ = 2.24 at 40 AGeV and 2.91 at 158 AGeV for Pb+Pb collisions, respectively (see Table 1 for the values of y_{beam} at different collision energies). In experiment, η_{peak} is obtained

Table 1: Beam rapidity, $y_{\text{beam}} = \ln \sqrt{s_{\text{NN}}}/m_p$, for various collision energies.

$\sqrt{s_{\text{NN}}}$ (GeV)	8.76	17.3	19.6	22.4	62.4	130	200	2760
Beam rapidity (y_{beam})	2.23	2.92	3.04	3.17	4.20	4.93	5.36	7.99

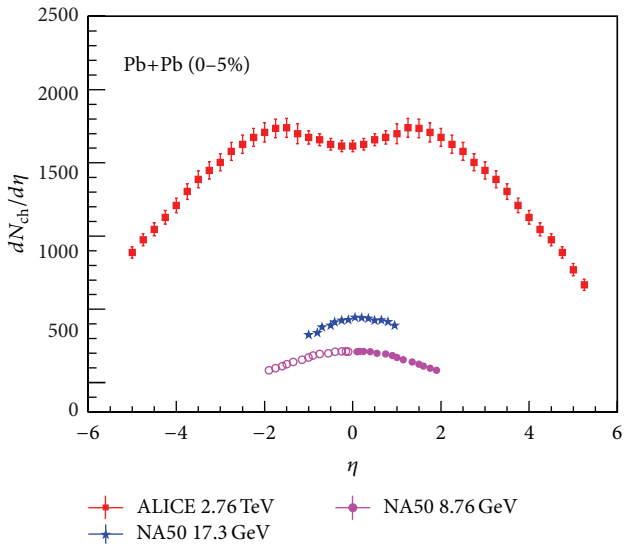

Figure 4: Charged particle pseudorapidity distributions of Pb+Pb collision systems for the most central events at different collision energies.

by fitting a Gaussian function to the $dN_{\text{ch}}/d\eta$ distribution. From the fitting, the η_{peak} comes out to be 2.43 and 3.12 for 40 AGeV and 158 AGeV, respectively. The hollow points at 40 AGeV correspond to the mirror reflection around the η_{peak}. The Pb+Pb data at 40 AGeV and 158 AGeV taken from NA50 have pseudorapidity coverage $(\eta - \eta_{\text{peak}}) < 1$ and $(\eta - \eta_{\text{peak}}) \leq 2$, respectively [10]. The $dN_{\text{ch}}/d\eta$ values of Pb+Pb collisions at $\sqrt{s_{\text{NN}}} = 2.76$ TeV are represented by squares and taken from ALICE experiment [11]. ALICE has more wider pseudorapidity coverage ($|\eta| < 5.25$). The data shown in Figures 2, 3, and 4 correspond to the most central events in the midrapidity. It is observed from Figures 2, 3, and 4 that the distribution is symmetric around $\eta = 0$. It is also found that with the increase of collision energy the width and amplitude of the $dN_{\text{ch}}/d\eta$ increase. Similarly, width of the central plateau region also increases with increase of energy. Moreover, the plateau region converts into a dip for Pb+Pb collisions at $\sqrt{s_{\text{NN}}} = 2.76$ TeV as shown in Figure 4. This can be addressed by the particles compositions which is directly related to the chemistry of the QGP. The pseudorapidity distribution of kaon has more dip than pion and proton has more dip than pion and kaons at $\eta = 0$. This is because of the mass of the particles. In another way, the heavier the particles are, the more the dip is in its pseudorapidity distribution [24]. This can be understood by looking into the transformation of rapidity to pseudorapidity variable and the corresponding spectra. The transformation is given by [25, 26]

$$\frac{dN}{d\eta} = J(\eta, p_T)\frac{dN}{dy}, \tag{4}$$

where the Jacobian $J(\eta, p_T)$ is given by

$$J(\eta, p_T) = \frac{p_T \cosh \eta}{\sqrt{m_0^2 + p_T^2 \cosh^2 \eta}}. \tag{5}$$

Hence it can be easily realized that at a fixed collision energy the higher is the mass of the particle, the lower is the value of the Jacobian. This translates to higher degree of dip in the pseudorapidity distribution. In the mean time, the transverse momentum spectra of identified particles show that the total proton+antiproton production cross section is higher at LHC than at RHIC [16]. This will increase the dip from RHIC to LHC energy. In contrast to this statement, the value of the Jacobian becomes smaller and smaller with increase in energy and approaches unity. For example, at the top RHIC energy $J = 1.25$ [27], whereas at $\sqrt{s_{\text{NN}}} = 2.76$ TeV, $J = 1.09$ [28]. Hence, only Jacobian seems to fail in explaining the observed dip in the pseudorapidity distribution. It should be noted here that at higher collision energies the observed dip in the pseudorapidity spectra of identified particles (produced secondaries) is the outcome of the interplay of fragmentation sources and midrapidity gluonic sources along with the effect of the Jacobian [29].

Landau hydrodynamical model predicts the pseudorapidity spectra of the produced particles to follow a Gaussian distribution [30]. However, later rapidity was used to characterize the particle production using Landau hydrodynamics by Carruthers and Duong-van [24]. Fitting a double Gaussian function to the pseudorapidity spectra is motivated by the trend of the data starting from SPS [31] to LHC [11] and the extracted width-parameter is used to study the dynamics of the system. Recently the ALICE experiment at LHC has used the following double Gaussian function to describe the multiplicity density of the charged particles [11]:

$$A_1 e^{-\eta^2/\sigma_1^2} - A_2 e^{-\eta^2/\sigma_2^2}. \tag{6}$$

It is reported in [11] that the values of $A_1/A_2, \sigma_1, \sigma_2$ are same within the errors for each measured centrality bin. To test this, whether it is valid for other systems and energies, we tried to fit this double Gaussian function to other multiplicity distributions of Au+Au and Cu+Cu systems measured at $\sqrt{s_{\text{NN}}} = 200$ and 130 GeV. To check the consistency, we considered $dN_{\text{ch}}/d\eta$ distributions of three centralities: 0–6%, 6–15%, and 15–25%. The χ^2 of the fitting, the fitting

Table 2: PHOBOS Cu+Cu 200 GeV.

Centrality (%)	χ^2/ndf	A_1	A_2	A_1/A_2	σ_1	σ_2
0–6	2.787/48	1130 ± 60.52	951.2 ± 56.7	1.19	2.94 ± 0.06	2.62 ± 0.08
6–15	1.238/48	821.7 ± 36.66	682.5 ± 36.67	1.20	3.0 ± 0.08	2.65 ± 0.09
15–25	0.913/48	789.9 ± 26.18	670.7 ± 525	1.18	3.02 ± 0.113	2.77 ± 0.12

Table 3: PHOBOS Au+Au 200 GeV.

Centrality (%)	χ^2/ndf	A_1	A_2	A_1/A_2	σ_1	σ_2
0–6	2.574/48	1987 ± 106	1461 ± 86.48	1.36	2.96 ± 0.04	2.28 ± 0.06
6–15	1.591/48	1831 ± 183.9	1344 ± 186.9	1.36	2.99 ± 0.08	2.42 ± 0.08
15–25	1.427/48	1488 ± 116.1	1125 ± 78.8	1.32	3.01 ± 0.50	2.53 ± 0.06

Table 4: PHOBOS Au+Au 130 GeV.

Centrality (%)	χ^2/ndf	A_1	A_2	A_1/A_2	σ_1	σ_2
0–6	4.987/48	1451 ± 132.1	904.8 ± 143.1	1.61	2.89 ± 0.06	2.04 ± 0.10
6–15	3.47/48	1128 ± 24.3	699.3 ± 88.9	1.61	2.97 ± 0.08	2.13 ± 0.08
15–25	1.674/48	898 ± 9.9	600 ± 60.7	1.51	2.99 ± 0.03	2.3 ± 0.08

parameters A_1, A_2, and the ratio of A_1/A_2, σ_1, σ_2 are given in Tables 2, 3, and 4. It can be seen from the tabulated values that the values of A_1/A_2, σ_1, σ_2 are same within the errors for different centralities at a particular energy. Hence, this observation for RHIC energies agrees with the observation made at LHC energy. It can be seen from Figures 2, 3, and 4 that with increase of energy the width of pseudorapidity distribution increases. This can be related to the longitudinal flow and velocity of sound of the system (c_s) using Landau hydrodynamic model. It is observed that with increase of energy, the velocity of sound increases and can be understood in the rapidity space as follows [32, 33]:

$$\sigma_y^2 = \frac{8}{3}\frac{c_s^2}{1-c_s^4}\ln\left(\frac{\sqrt{s_{\mathrm{NN}}}}{2m_p}\right), \tag{7}$$

where m_p is mass of proton and σ_y is the width of rapidity distribution of charged particles and c_s^2 is the square of the velocity of sound, which equals 1/3 for an ideal gas.

3.2. Longitudinal Scaling. Charged particle production in the higher rapidity region is subject of interest in terms of hypothesis of limiting fragmentation [34]. According to this hypothesis, the observed pseudorapidity density of particle as a function of $\eta' = \eta - y_{\mathrm{beam}}$ approaches a limiting value in the fragmentation region even if the colliding energy is increased. Here $y_{\mathrm{beam}} = \ln(\sqrt{s_{\mathrm{NN}}}/m_p)$. This can be explained by considering the whole heavy-ion collision process in laboratory frame of one of the nuclei. The hypothesis can be represented as follows. In the laboratory frame, out of the produced particles, some of them will have velocity increasing with the increase of collision energy. But some of them will have fixed velocity (or pseudorapidity) as collision energy increases which is postulated as they have approached a limiting distribution. This can be explained as follows. In the frame of the target nucleus, the projectile is Lorentz contracted and appears like a disk, collides, and produces particles. As colliding energy is increased, the target will observe that a more contracted disk is colliding with it. However, the momentum transfer process between the projectile and target does not change with respect to the contraction rate. This leads to the limiting distribution of produced particles in the fragmentation region even if the collision energy is increased. One of the advantages of this observation is that it can be seen both in rapidity and in pseudorapidity distributions of the particles because at large forward rapidity region, $\eta \sim y - \ln(p_T/m_T)$.

The normalized charged particle multiplicity density per participant pair as a function of $\eta' = \eta - y_{\mathrm{beam}}$ for different collision systems and different energies is shown in Figures 5, 6, and 7. In Figure 5, the data are shown for Cu+Cu collisions at $\sqrt{s_{\mathrm{NN}}}$ = 22.4 GeV, 62.4 GeV, and 200 GeV [22]. In Figure 6, the data are shown for Au+Au collisions at $\sqrt{s_{\mathrm{NN}}}$ = 19.6 GeV, 62.4 GeV, 130 GeV, and 200 GeV [9, 23]. Similarly, in Figure 7, the data are shown for Pb+Pb collisions at beam energies of 40 AGeV, 158 AGeV and at $\sqrt{s_{\mathrm{NN}}}$ = 2.76 GeV [10, 11]. The charged particle numbers for Pb+Pb collisions at $\sqrt{s_{\mathrm{NN}}}$ = 2.76 TeV at forward rapidity are estimated by extrapolating the double Gaussian function used to explain the charged particle distribution [11]. Figures 5, 6, and 7 show the saturation or limiting nature of charged particle density at very high value of $\eta - y_{\mathrm{beam}}$ even if the energy of the projectile is increased. It is also observed in high energy $e^+ + e^-$, $p + p$, and d + Au collisions [35–37]. The hypothesis of limiting fragmentation assumes that the hadronic cross section approaches an asymptotic value at high energy [38]. That means the hadronic excitation and breakup probability are almost independent of projectile energy. But later it is found that the hadronic cross section increases with increase of center of mass energy. The most spectacular fact of this

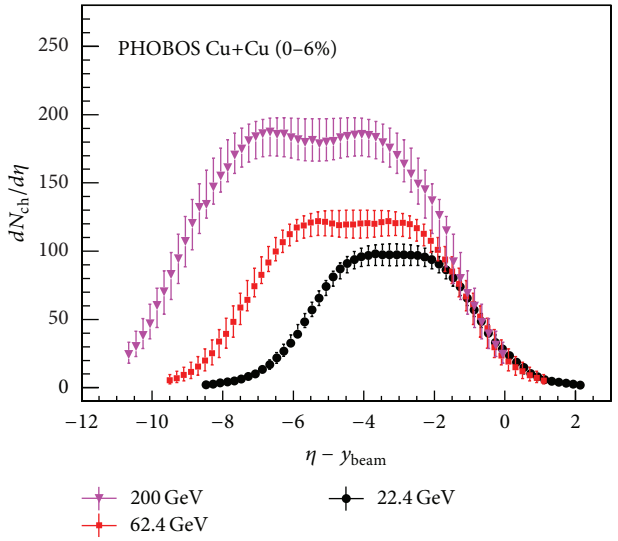

FIGURE 5: Charged particle multiplicity density normalized by participant pairs for Cu+Cu collisions at different energies, shown in the projectile rest frame by using $\eta' = \eta - y_{beam}$.

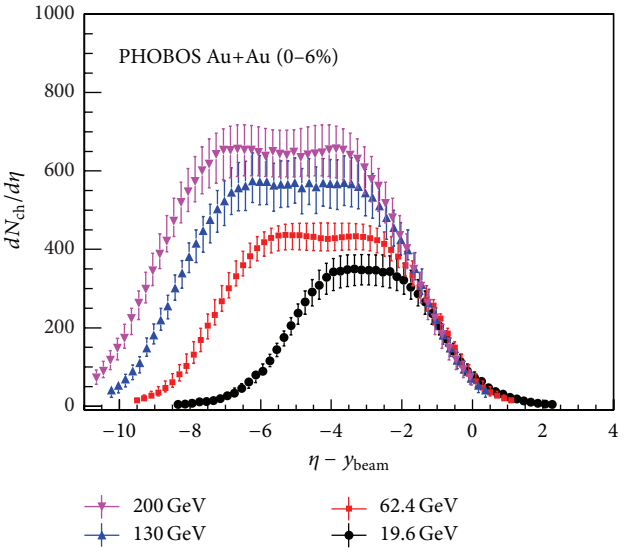

FIGURE 6: Charged particle multiplicity density normalized by participant pairs for Au+Au collisions at different energies, shown in the rest frame of projectile by using $\eta' = \eta - y_{beam}$.

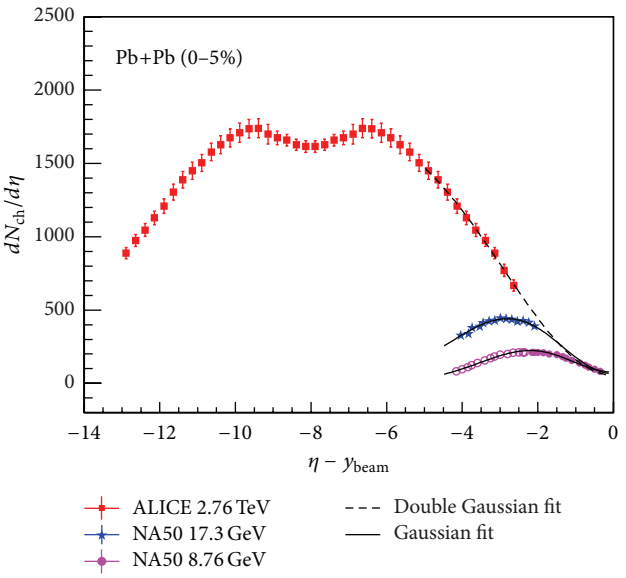

FIGURE 7: Charged particle multiplicity density normalized by participant pairs for Pb+Pb collisions at different energies, shown in one of the rest frames of the projectile by using $\eta' = \eta - y_{beam}$.

hypothesis is that still this phenomenon is observed for a wide range of collision energies. Later this limiting fragmentation was tried to explain through Color Glass Condensate (CGC) model [39, 40]. The gluon saturation picture at very small x is used to understand this phenomenon. The charged particle multiplicity density normalized to participant pair obtained from CGC model is compared with the RHIC data at different energies [39, 40]. This CGC based model calculation provides reasonable description of the data at the fragmentation region for $p+p$ and $A+A$ collisions systems by considering different scale parameters and initial conditions. However, more precise modelling of the impact parameter dependence of the "unintegrated" gluon distribution functions is demanded in these models. In addition to this, the precise estimation of final state effects and inclusion of quark distributions into this frameworks are needed to explain the whole spectrum of data.

In the framework of statistical thermal model, the extended longitudinal scaling can be explained up to RHIC energies [41]. It is also predicted that the LHC data will not show the longitudinal scaling, which is supported by the string percolation model [42]. However, the recent LHC data violate the predictions from thermal model and follow the universal longitudinal scaling. It indicates that at LHC some nonequilibrium phenomenon may be playing a role, which needs to be understood [43].

It is reported in [23] that the shape of the scaled pseudorapidity density in the rest frame of the projectile is independent of the beam energy. However, this shape differs when it is studied as a function of different centralities. This centrality dependence is mainly because of an excess of particles at higher η and narrowing of the width of the pseudorapidity distribution in peripheral $A+A$ collisions. The excess particles basically originate from nuclear remnant in the peripheral collisions. So it is realized that the shape is mainly a function of collision geometry. To cancel out the geometry effect, it is argued in [9, 23] that ratio of $dN_{ch}/d\eta$ normalized to N_{part} of central to peripheral events (R_{PC}) can be used to ensure the observations on the energy-independence of the shape called longitudinal scaling in the forward rapidities. The variable R_{PC} is defined as [23]

$$R_{PC}\left(\eta', 35\text{–}45\%\right) = \frac{\left(dN_{ch}/d\eta\right)^{35\text{–}45\%}/N_{part}^{35\text{–}45\%}}{\left(dN_{ch}/d\eta\right)^{0\text{–}6\%}/N_{part}^{0\text{–}6\%}}. \quad (8)$$

It was introduced to show the energy independence behaviour for Au+Au collisions at $\sqrt{s_{NN}}$ = 19.6, 130, and

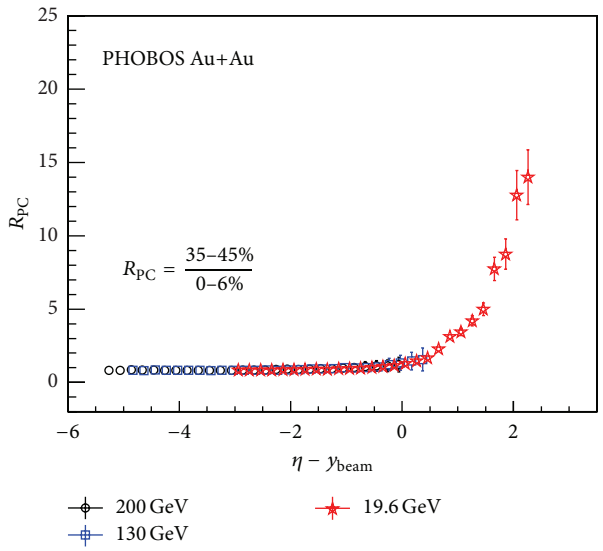

FIGURE 8: R_{PC} as a function of $\eta' = \eta - y_{beam}$ for Au+Au collisions at different energies.

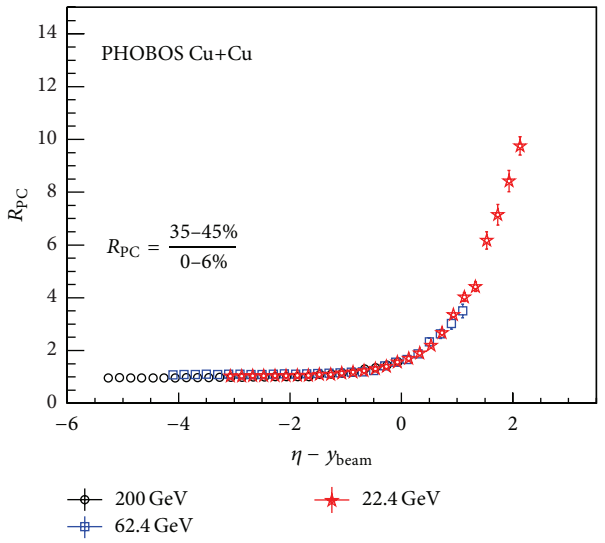

FIGURE 9: R_{PC} as a function of $\eta' = \eta - y_{beam}$ for Cu+Cu collisions at different energies.

200 GeV. This is shown in Figure 8 [23]. The R_{PC} as a function of $\eta - y_{beam}$ for Cu+Cu collisions at $\sqrt{s_{NN}}$ = 22.4, 62.4, and 200 GeV are shown in Figure 9 [22]. Similarly, in Figure 10, values of R_{PC} of Pb+Pb collisions at beam energies of 40 AGeV, 158 AGeV and $\sqrt{s_{NN}}$ = 2.76 TeV are shown. Very interestingly, we observe that for both Au+Au (Figure 8) and Cu+Cu (Figure 9) collision data, R_{PC} is found to be independent of collision energy. For Pb+Pb collisions at 2.76 TeV, the peripheral events correspond to 30–40% centrality and central events of 0–5% centrality [11]. For 158 AGeV and 40 AGeV Pb+Pb collisions, peripheral events correspond to 25–35% centrality and central events correspond to 0–5% centrality [10]. From Figure 10, it is difficult to conclude about the Pb+Pb collision data for the three energies as the data are not available for the whole pseudorapidity range as far as this discussion is concerned. However, the trend of the R_{PC} values as a function of $\eta - y_{beam}$ in Figure 10 goes in line with the observations at RHIC.

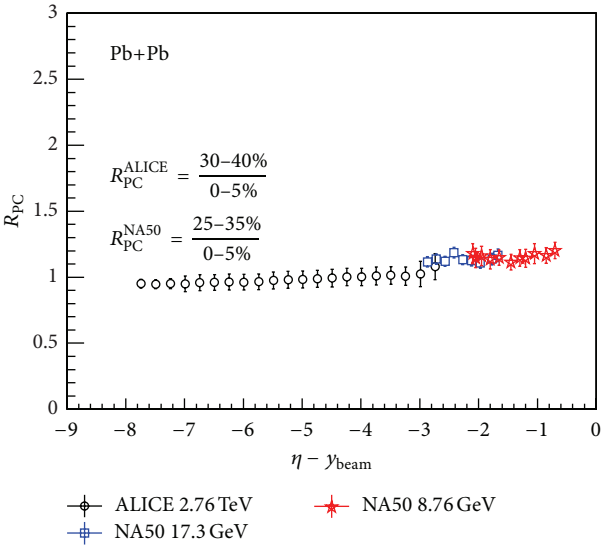

FIGURE 10: R_{PC} as a function of $\eta' = \eta - y_{beam}$ for Pb+Pb collisions at three different energies.

3.3. Factorization. In a typical heavy-ion collision process, the nucleons in the overlap zones are called participant nucleons which must have suffered at least one inelastic collision. Hence, the charged particles produced in the collision may have some relation with the number of participant nucleons in the reaction zone as well as the number of binary collisions. A nucleus-nucleus collision can be thought of superposition of many individual $p + p$ collisions. So the final charged particle density should have some empirical relationship with the $\langle N_{part} \rangle$ and number of binary collisions (N_{coll}). In the framework of "wounded nucleon model" [44], it is observed that the $dN_{ch}/d\eta$ scales with some power of N_{part} up to the SPS energy [8]. That is called power law fit and is given by

$$\frac{dN_{ch}}{d\eta} \propto N_{part}^{\alpha}, \tag{9}$$

where α is found to be ~1 for SPS energies. This linear relation with N_{part} is interpreted as that the particle production up to SPS energies is mainly from the soft processes. However, the particle multiplicity at RHIC energies could not be explained by the above relationship. Then a two-component model was adopted which incorporates both the contribution of soft and hard processes by considering the $\langle N_{part} \rangle$ and $\langle N_{coll} \rangle$ to describe the final state hadron multiplicity [8, 45]. The two-component model is given as

$$\frac{dN_{ch}}{d\eta} = (1 - x)\, n_{pp} \frac{\langle N_{part} \rangle}{2} + x n_{pp} \langle N_{coll} \rangle, \tag{10}$$

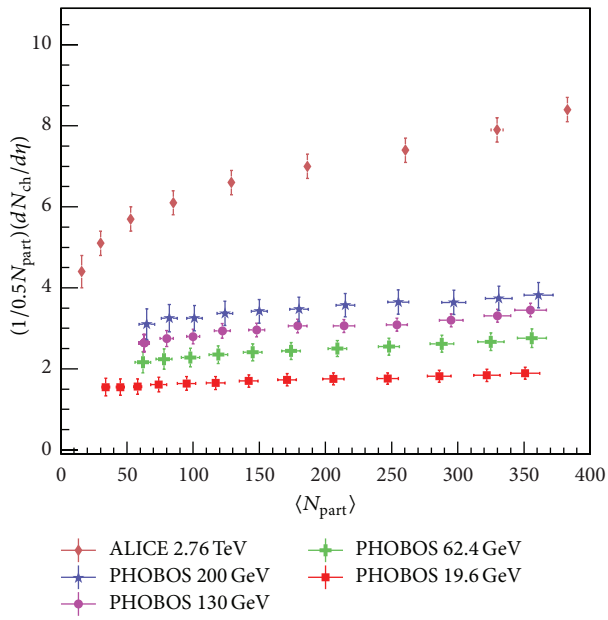

FIGURE 11: N_{part} normalized charged particle density for different collision energies.

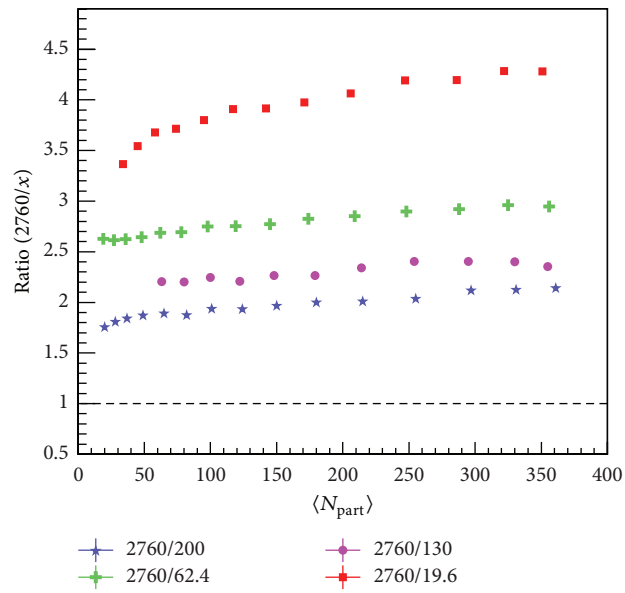

FIGURE 12: Ratio of charged particle density for different energies normalized per participant pair as a function of collision centrality.

where n_{pp} is the measured multiplicity density in $p + p$ collisions due to x fraction of hard processes and $(1 - x)$ fraction represents the soft process.

Number of binary collisions is proportional to nucleon-nucleon inelastic cross section (σ_{inel}^{NN}). With increase of collision energy, the σ_{inel}^{NN} also increases [38]. This results in dramatic increase of N_{coll} with the increase of collision energy and therefore the contribution of hard process will be dominant for particles production. So it is expected that there will be a strong centrality dependence of pseudorapidity distributions at higher energies. This can be tested by taking the ratio of scaled yield at the respective centralities at different energies. It is reported in [12, 13] that the centrality dependence of particle production in the midrapidity exhibits factorization of beam energy and collision centrality as follows:

$$\frac{2}{\langle N_{part}\rangle}\frac{dN_{ch}}{d\eta} = f(s)\, g\left(N_{part}\right). \tag{11}$$

Equation (11) basically illustrates the energy-centrality factorization. In the right hand side of (11), the first term, that is, $f(s)$, depends on the energy and the second term, that is, $g(N_{part})$, depends on the $\langle N_{part}\rangle$. In the midrapidity, the charged particle multiplicity density normalized to the participant pair ($\langle N_{part}\rangle/2$) at different energies is shown in Figure 11. The collision data are fitted with the parametrized form of right hand side of (11). For Au+Au collision, the parametrized forms of $f(s)$ and $g(N_{part})$ found from [13] are as follows:

$$\begin{aligned} f(s) &= 0.0147\,[\ln(s)]^2 + 0.6, \\ g\left(N_{part}\right) &= 1 + 0.095N_{part}^{1/3}. \end{aligned} \tag{12}$$

Similarly, for Cu+Cu collisions, the coefficients of $f(s)$ do not change. However, the coefficient of $N_{part}^{1/3}$ in $g(N_{part})$ changes, which is given by

$$g\left(N_{part}\right) = 1 + 0.129N_{part}^{1/3}. \tag{13}$$

In Figure 12, ratios of the charged particle multiplicity density normalized to the participant pair of Pb+Pb collisions at $\sqrt{s_{NN}} = 2.76$ TeV and Au+Au collisions data at different energies are shown as a function of $\langle N_{part}\rangle$. This observation implies that the pseudorapidity density of particles in the midrapidity normalized per participant pair can be factorized. However, when the collision system changes, the $N_{part}^{1/3}$ dependence comes into picture. We tried to fit the parametrized form of (11) with the LHC data. We keep the form of $f(s)$ the same and set one parameter free of $g(N_{part})$. However, it does not fit the data. This is shown in Figure 13. Contrary, when both of the parameters of (11) are set free, then it fits well to the data. This observation contradicts the observation at RHIC. The RHIC data show that only the coefficient of $N_{part}^{1/3}$ changes when collision system changes at the same collision energy. However, at LHC energy, the energy as well as the system size changes. After χ^2 minimization, for better fit, we get the following form of $g(N_{part})$ for LHC data. It can be inferred that some other factor is playing a role for the particle production at LHC energy in addition to the RHIC energy:

$$g\left(N_{part}\right) = 0.833 + 0.142N_{part}^{1/3}. \tag{14}$$

3.4. Expansion Dynamics. The space-time evolution of the fireball created in the heavy-ion collisions can be explained by relativistic hydrodynamical approach which assumes that the

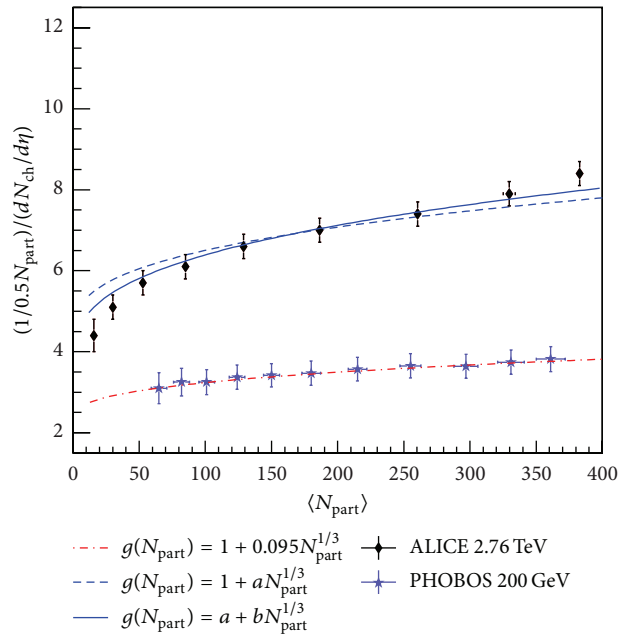

FIGURE 13: Factorization of RHIC and LHC data. The data points are fitted with various parametrized forms of (11).

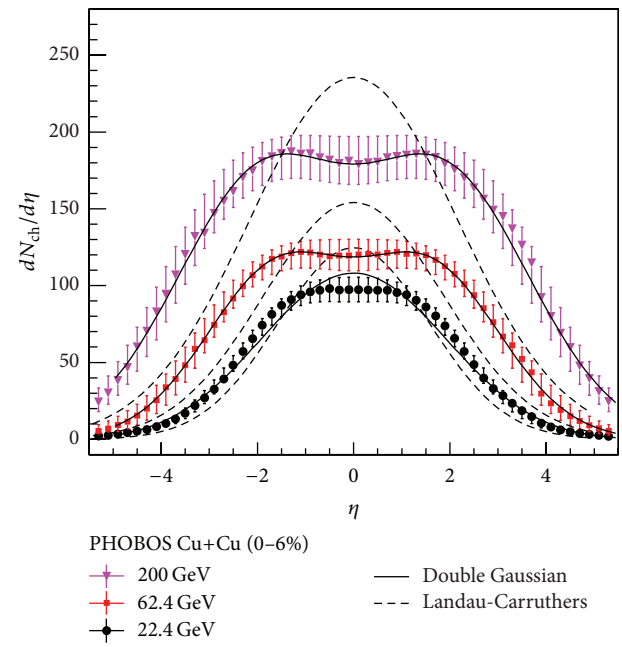

FIGURE 14: The charged particle multiplicity density distributions of Cu+Cu collisions at three different energies, fitted with double Gaussian function and Landau-Carruthers functions.

medium is continuously flowing. The elliptic flow measurements, the two-particle correlations, and transverse momentum spectra results at RHIC have given ample evidence of a strongly interacting medium created in the laboratory. There are many proposed statistical as well as hydrodynamical models in the past to explain the multiplicity and expansion dynamics of the systems. Landau hydrodynamic model is one of them, which is widely used to explain the expansion of the system produced in the collision, like $e^+ + e^-$, $p + p$, and $A + A$ [30]. It has successfully explained the low energy collision data including the charged pion data at RHIC [46, 47]. The form of Landau hydrodynamics has been evolved with time to explain the global particle multiplicity and the differential rapidity distribution [24, 48]. The width of the charged particle density distribution in the midrapidity can shed some light on the longitudinal expansion dynamics of the system, velocity of sound, and initial and final state rescattering. A detailed analysis about these is given in [49]. It can also be used to define the degree of stopping or transparency in the heavy-ion collision reactions.

According to Landau hydrodynamics, the number distribution of produced particles is given by [30, 50]

$$\frac{1}{N}\frac{dN}{d\lambda} = \frac{\exp\left(-\lambda^2/2L\right)}{(2\pi L)^{1/2}}, \tag{15}$$

where $\lambda = -\ln\tan(\theta/2) \equiv \eta$ and $L = \ln\gamma = (1/2)\ln(s/4m^2)$, which gives a measure of the thickness of the Lorentz contracted disks of the colliding hadronic matter. Here, m is the mass of the proton, m_p, and $\gamma = \sqrt{s_{\text{NN}}}/2m_p$ is the Lorentz contraction factor. Later, instead of pseudorapidity, the rapidity variable was used by Carruthers and Duong-van to describe the production of the secondaries in high energy interactions [24]. The Gaussian form of which is given as

$$\frac{dN}{dy} \propto \exp\left(-\frac{y^2}{2L}\right). \tag{16}$$

Additionally, later in [48], the pseudorapidity variable is substituted by rapidity to describe the distribution appropriately (the rapidity distribution of charged particles differs from pseudorapidity distribution at the smaller rapidity region and a detailed discussion is made previously in this review). Then the rapidity distribution is given as [48]

$$\frac{dN}{dy} \propto \exp\left(\sqrt{y_b^2 - y^2}\right), \tag{17}$$

where the beam rapidity, y_b, in the center of mass frame is $\cosh^{-1}(\sqrt{s_{\text{NN}}}/2m_p) = \ln(\sqrt{s_{\text{NN}}}/m_p)$. Then [48] connects the total entropy of the system with the number density such that their ratio is constant for a thermally equilibrated system.

It is found that when the transformation of the distribution is made to rest frame of one of the colliding nuclei, the Gaussian form as given in (14) shows the limiting fragmentation behaviour. And surprisingly, by setting some parameters, it also matches multiplicity distributions with the CGC calculations [46].

In this review, we have tried to see the agreement of pseudorapidity distributions of charged particles by Landau-Carruthers function. The advantage of fitting Landau-Carruthers form to the data is that the λ variable used in the function has similar form as the pseudorapidity. The multiplicity distribution of Cu+Cu collision data as a function of rapidity for different energies is shown in Figure 14.

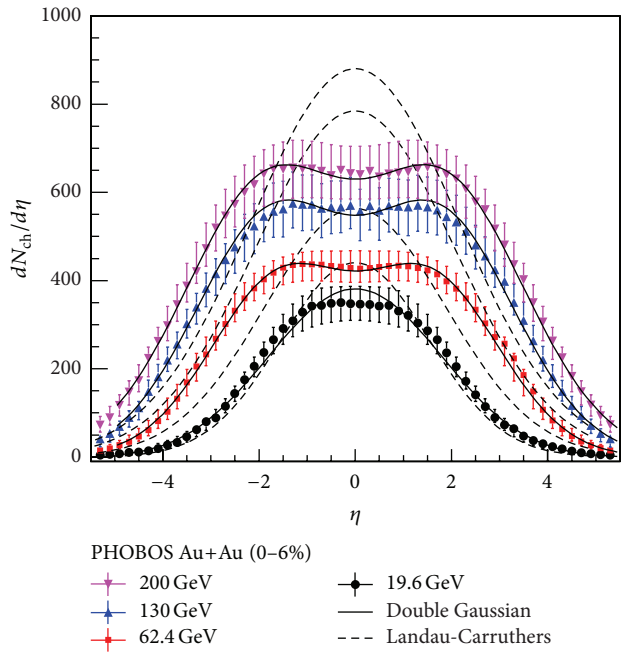

Figure 15: The charged particle multiplicity density distributions of Au+Au collisions at three different energies, fitted with double Gaussian function and Landau-Carruthers functions.

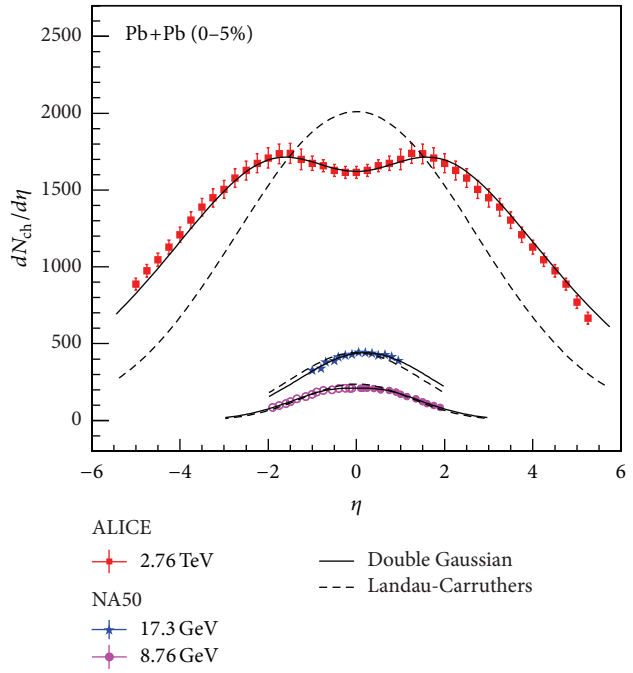

Figure 16: The charged particle multiplicity density distributions of Pb+Pb collisions at three different energies, fitted with double Gaussian function and Landau-Carruthers functions.

The Cu+Cu collision data are fitted with the Landau-Carruthers functions. The multiplicity distribution of Au+Au collisions as a function of rapidity for different energies is shown in Figure 15. Similarly, the rapidity distributions of charged particles of Pb+Pb collisions at different energies are shown in Figure 16. The $dN_{ch}/d\eta$ distribution of charged particles is also fitted with double-Gaussian functions. The width of the distributions obtained from the data and the models are divided and shown as a function of collision energy in Figure 17. It is observed from Figure 17 that Landau-Carruthers hydrodynamics explains the data starting from AGS, SPS to RHIC as the ratio is closed to one. So far the shape of pseudorapidity distribution of the charged particles at LHC is concerned, Landau hydrodynamics seems to deviate from the trend of the data.

3.5. Energy Dependence of Multiplicity Density. The energy dependence of charged particle multiplicity density distribution per participant pair for most central collisions in heavy-ion collisions at midrapidity and for nucleon-nucleon nonsingle diffractive (NSD) and inelastic (INEL) collisions as a function of collision energy is shown in Figure 18. The data points are from different energy and different collision species. To explain the normalized particle distribution in the midrapidity, different phenomenological functions are fitted. Up to top RHIC energy $dN_{ch}/d\eta$ for heavy-ion collisions is well described by a logarithmic function. However, the LHC data is underestimated by logarithmic function up to 26%. On the other hand, a power law fit seems to overestimate the low energy data for nucleus-nucleus collisions while explaining the high energy data up to LHC energies. Looking

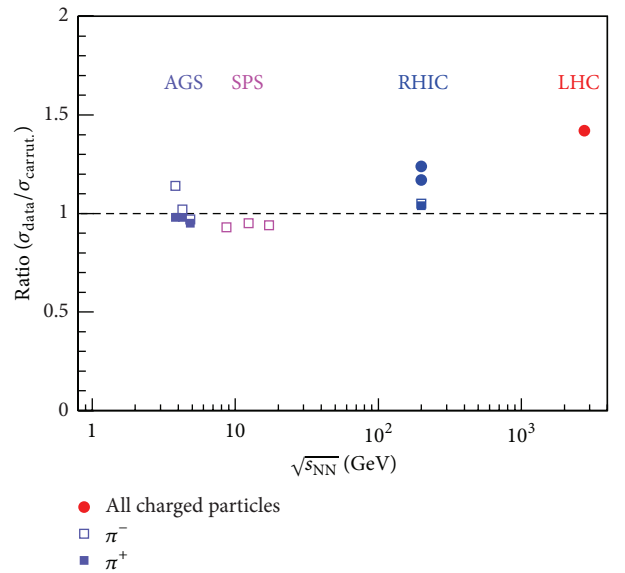

Figure 17: The ratio of the widths of the data to the width obtained by fitting Landau-Carruthers function to the charged particle multiplicity density, as a function of collision energy.

at the low-energy and high-energy behaviours of charge particle production being well-described by a logarithmic function and power-law functions, respectively, we have tried to fit a hybrid function (a combination of both) and find a very good agreement with the nucleus-nucleus data at all energies up to LHC 2.76 TeV. The physics motivation of the hybrid function can be explained by considering the result by

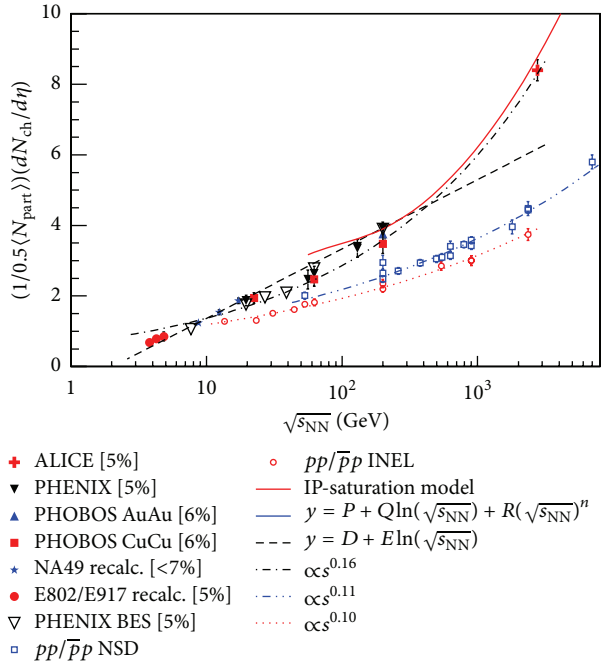

FIGURE 18: Energy dependence of charged particle multiplicity density distribution per participant pair for most central collisions at midrapidity. Compared are the corresponding measurements in $p + p/p + \overline{p}$ NSD and INEL collisions.

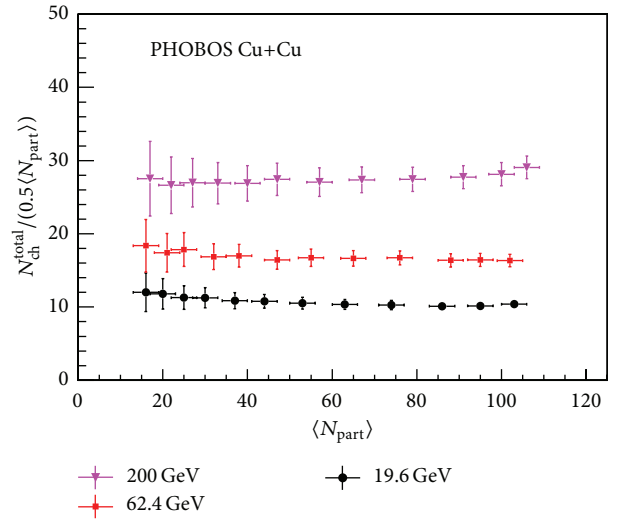

FIGURE 19: $N_{\rm ch}^{\rm total}$ normalized to participant pair as a function of $N_{\rm part}$ for Cu+Cu collisions at different collision energies.

Wolschin et al. which states that at high energy charged particle multiplicity can be explained by a combination of midrapidity gluonic source predicted by the power law function and a fragmentation source predicted by logarithmic function [29, 51]. The predictions from IP-saturation model [52] for the top RHIC energy and higher are also shown for a comparison with the corresponding nucleus-nucleus experimental data.

For a direct comparison with $A + A$ data, we have put together the $p + p(\overline{p})$ NSD and INEL data. Both data seem to fit to a power-law behaviour with the power decreasing while going from $A+A$ to $p+p(\overline{p})$ collisions. This is in an agreement with the results obtained by considering the $A + A$ and $p + p(\overline{p})$ bulk data in the framework of constituent quark picture [43, 53–60]. The model which combines the constituent quark picture and Landau hydrodynamics has been proposed in [53, 60], where the universality of the bulk production in e^+e^-, $p + p(\overline{p})$ and $A + A$ has been demonstrated. Within this model, the process of particle production is driven by the amount of energy deposited by interacting participants into the small Lorentz-contracted volume during the early stage of the collision. The whole process of a collision is then considered as the expansion and the subsequent break-up into particles from an initial state. This makes the secondary particle production be basically driven by the amount of the initial effective energy deposited by participants quarks or nucleons, into the Lorentz contracted overlap region. In $p + p(\overline{p})$ collisions, a single constituent (or dressed) quark from each nucleon takes part in a collision and rest are considered as spectators. Thus, the effective energy for the production of secondary particles is the energy carried by a single quark pair, that is, 1/3 of the entire nucleon energy. In contrary, in the head-on heavy-ion collisions, the participating nucleons are considered colliding by all three constituent quarks from each nucleon which makes the whole energy of the colliding nucleons (participants) available for secondary particle production. Thus, one expects bulk observables measured in the head-on heavy-ion collisions at the center of mass energy per nucleon, $\sqrt{s_{\rm NN}}$, to be similar to those from $p + p(\overline{p})$ collisions but at a three times larger center of mass energy; that is, $\sqrt{s_{pp}}/3 \approx \sqrt{s_{\rm NN}}$. Using this model, it has been shown [53, 60] that the multiplicity and the midrapidity center of mass energy behaviour measured in nuclear collisions are well reproduced from the $p + p(\overline{p})$ measurements in the $\sqrt{s_{\rm NN}}$ energy range from a few GeV up to the top RHIC energy. In [47] it is shown that based on this model the midrapidity density $\sqrt{s_{\rm NN}}$-dependence is well described up to a few TeV LHC data. Moreover, in the effective energy terms, the midrapidity density $N_{\rm part}$ dependence is well described for RHIC and for the LHC data shown to complement the energy dependence of heavy-ion data.

3.6. Scaling of N_{ch}^{total} with N_{part}. It is observed that the particle multiplicity at midrapidity does not scale with the number of participant nucleons, that is, $N_{\rm part}$. It is observed from [9, 13] that the total charged particle measured over a wide range of pseudorapidity, when normalized per participant pair, scales with $N_{\rm part}$. We considered different collision energies and collision systems to see the scaling behaviour of total charged particles. The normalized $N_{\rm ch}^{\rm total}$ per participant pair as a function of $N_{\rm part}$ are shown in Figures 19 and 20 for Cu+Cu and Au+Au collisions, respectively. The error bars shown in the figures are statistical only.

It is observed from Figures 19 and 20 that the participant pair normalized $N_{\rm ch}^{\rm total}$ scales perfectly with $N_{\rm part}$ within the statistical uncertainties. For both Cu+Cu and Au+Au

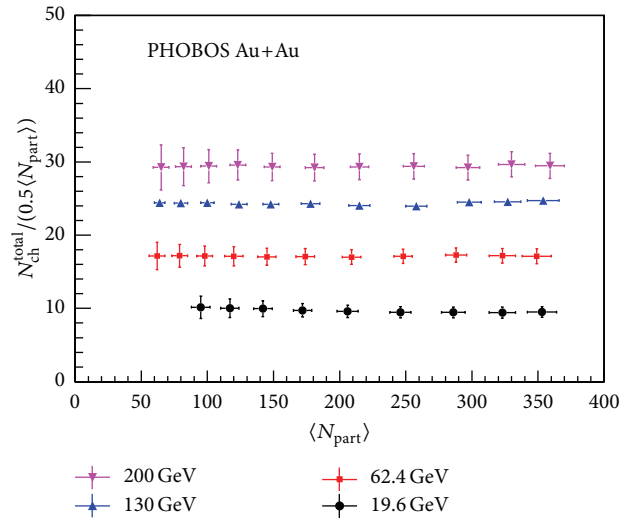

FIGURE 20: N_{ch}^{total} normalized to participant pair as a function of N_{part} for Au+Au collisions at different collision energies.

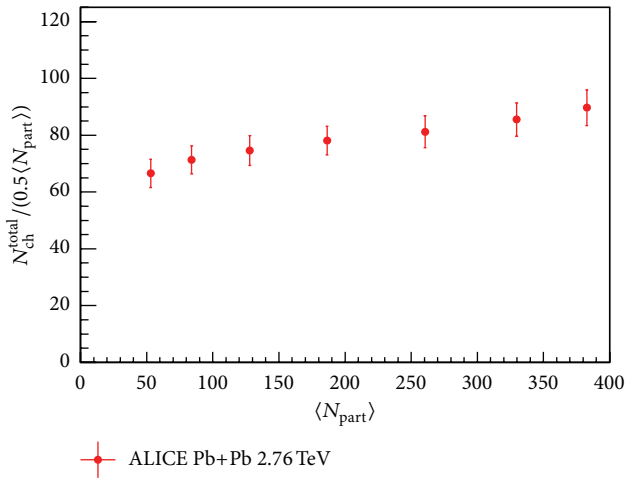

FIGURE 21: N_{ch}^{total} normalized to participant pair as a function of N_{part} for Pb+Pb collisions at $\sqrt{s_{NN}} = 2.76$ TeV.

systems, the normalized value of N_{ch}^{total} with respect to N_{part} is constant as a function of N_{part} and increases with increase of collision energy. It implies that modifications to particle production at forward rapidities are strongly correlated with compensating changes at midrapidity. However, similar effect was not observed for Pb+Pb collisions at $\sqrt{s_{NN}} = 2.76$ TeV, as shown in Figure 21. The monotonic increase of N_{ch}^{total} with centrality is because of the increased gluonic contributions in the midrapidity region [29, 51] and hence a participant scaling is violated. This needs further theoretical understanding along with the availability of higher energy data.

3.7. Energy Dependence of N_{ch}^{total}. As discussed earlier, the total charged particles normalized per participant pair ($N_{ch}^{total}/0.5\langle N_{part}\rangle$) for Cu+Cu, Au+Au systems at different collision energies are independent of centrality. In addition

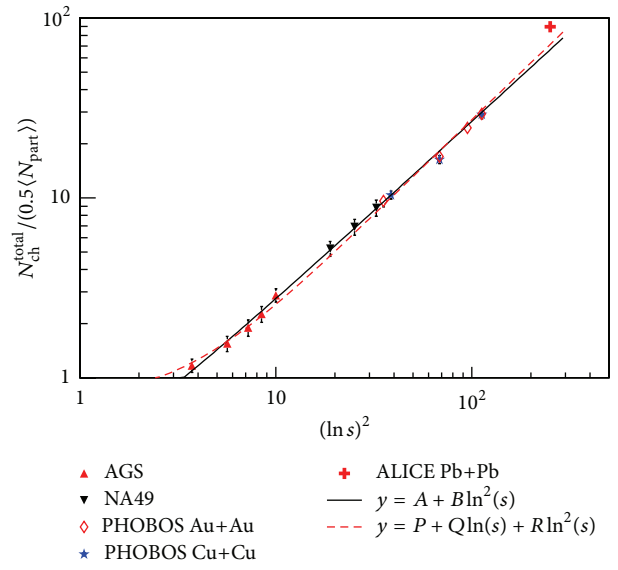

FIGURE 22: Energy dependence of total charged particle multiplicity per participant pair for most central collisions.

to this, the N_{ch}^{total} value increases with increase of energy for all centralities. The energy dependence of N_{ch}^{total} from AGS to LHC is shown in Figure 22. It is observed that the $dN_{ch}/d\eta$ distribution in the midrapidity is almost flat [13] and the width of the distribution decreases with decrease of collision energy. The fragmentation region can be explained by $dN_{ch}/d\eta = \alpha(y_{beam} + \eta_0 - \eta)$. So the overall $dN_{ch}/d\eta$ distribution now can be thought of as a trapezoid and hence the total charged particles can be given by the trapezoidal rule as follows [13]:

$$N_{ch}^{tpz} = \frac{dN_{ch}|_0}{d\eta}\left(2\eta_0 + 2y_{beam} - \frac{\langle N_{part}\rangle}{2\alpha}\frac{dN_{ch}|_0}{d\eta}\right). \quad (18)$$

As $y_{beam} \simeq (1/2)\ln s_{NN} - \ln(m_0c^2)$ for $\sqrt{s_{NN}} \gg m_0$, m_0 being the mass of the nucleon, (18) reduces to

$$\frac{N_{ch}^{tpz}}{0.5\langle N_{part}\rangle} \simeq A + B\ln s_{NN} + C(\ln s_{NN})^2. \quad (19)$$

To explain the evolution of $N_{ch}^{total}/(0.5\langle N_{part}\rangle)$ with respect to $\sqrt{s_{NN}}$, parametrized form of (19) is used and fitted with the collision data which is shown by a dashed line in Figure 22. It is found that this equation explains the PHOBOS Cu+Cu and Au+Au data at RHIC. However, it fails to explain the data at lower energies. Only after considering the leading term $(\ln s_{NN})^2$ in (19), it explains the whole spectrum of energy dependence of total charged particles very nicely starting from $\sqrt{s_{NN}} = 2.4$ GeV to $\sqrt{s_{NN}} = 200$ GeV. The general form is

$$\frac{N_{ch}^{tpz}}{0.5\langle N_{part}\rangle} = A + C(\ln s_{NN})^2. \quad (20)$$

The fitting of (20) to the data point is shown in Figure 22 by the solid line. It can be seen from Figure 22 that derived form

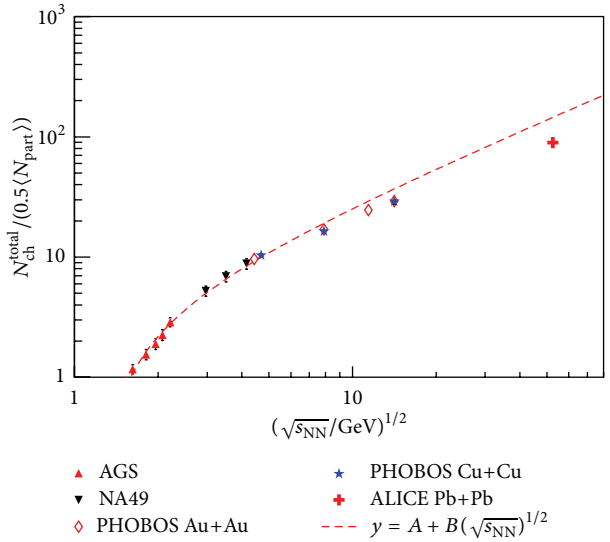

FIGURE 23: Total charged particle multiplicity per participant pair as a function of $(\sqrt{s_{NN}}/\text{GeV})^{1/2}$. The data points are fitted with the parametrized form of (21), which is shown by the dotted line.

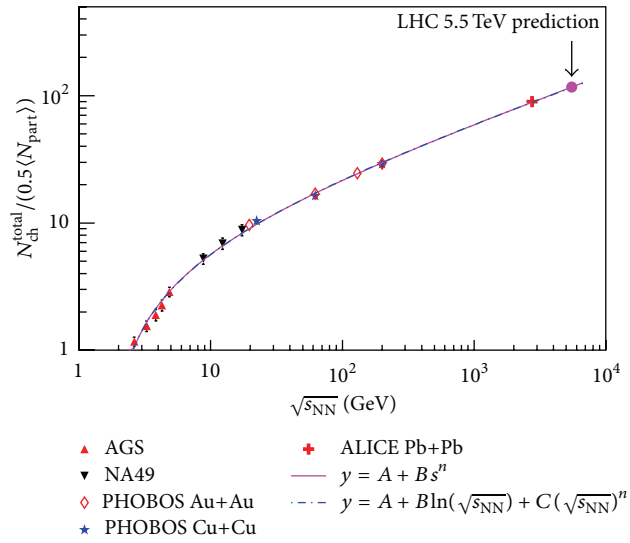

FIGURE 24: Total charged particle multiplicity per participant pair as a function of $\sqrt{s_{NN}}$. The data points are fitted with the parametrized form of (24), which is shown by the dotted line. The continuous line shows a comparison with a power law form of energy dependence.

of trapezoidal rule given by (19) and (20) underestimates the N_{ch}^{total} of Pb+Pb collisions at $\sqrt{s_{NN}} = 2.76$ TeV measured by the ALICE experiment. This is because the $dN_{ch}/d\eta$ distribution of Pb+Pb data has a dip which in principle deviates from a trapezoidal shape.

Measuring N_{ch}^{total} as a function of $(\sqrt{s_{NN}})^{1/2}$ is important in terms of Landau hydrodynamics. According to Landau hydrodynamics, the ratio of entropy density to the number density for a thermally equilibrated system is constant. In other words, the number density is proportional to the entropy density and hence the total number of particles is proportional to the total entropy. To be noted here that during the hydrodynamic expansion of the system, the total entropy remains constant. So by measuring the total observed particles, the initial entropy can be determined and vice versa. For a system which is in local thermal equilibrium, the entropy density is proportional to the energy density and, under this assumption, we can arrive at this relationship of N_{ch}^{total} with respect to the center of mass energy $\sqrt{s_{NN}}$ as follows [48]:

$$\frac{N_{ch}^{total}}{0.5\langle N_{part}\rangle} = K\left(\sqrt{s_{NN}}/\text{GeV}\right)^{1/2}. \quad (21)$$

The parametrized form of (21) is obtained for PHOBOS Au+Au data, which is given by [48]

$$\frac{N_{ch}^{total}}{0.5\langle N_{part}\rangle} = 1.135 + 2.019\left(\sqrt{s_{NN}}/\text{GeV}\right)^{1/2} \quad (22)$$

and in general can be written as

$$\frac{N_{ch}^{total}}{0.5\langle N_{part}\rangle} = \text{A} + \text{B}\left(\sqrt{s_{NN}}/\text{GeV}\right)^{1/2}. \quad (23)$$

We have tried to fit (23) to the $N_{ch}^{total}/(0.5\langle N_{part}\rangle)$ data as a function of $(\sqrt{s_{NN}}/\text{GeV})^{1/2}$ obtained from AGS to LHC experiments which is shown by the dotted line in Figure 23. It is observed that (23) fails to explain the LHC data, as it overpredicts the corresponding value at LHC. This observation goes in line with the measurement as shown in Figure 17; that is, the width of $dN_{ch}/d\eta$ of Pb+Pb data at $\sqrt{s_{NN}} = 2.76$ TeV is more than the expectation of Landau hydrodynamics. It is seen that the hybrid function nicely describes the whole $dN_{ch}/d\eta$ distribution as a function of $\sqrt{s_{NN}}$ and Landau hydrodynamics cannot explain the LHC data. With this motivation, we tried to fit a hybrid form as given in (24) to fit the $N_{ch}^{total}/(0.5\langle N_{part}\rangle)$ as a function of $\sqrt{s_{NN}}$ [43]:

$$\frac{N_{ch}^{total}}{0.5\langle N_{part}\rangle} = \text{A} + \text{B}\ln\left(\sqrt{s_{NN}}\right) + \text{C}\left(\sqrt{s_{NN}}\right)^n. \quad (24)$$

It is found that this hybrid function can explain the whole range of the data up to the LHC energy as shown in Figure 24. The extrapolation of this function for the upcoming LHC Pb+Pb collisions at $\sqrt{s_{NN}} = 5.5$ TeV is shown by the filled circle in Figure 24.

4. Pseudorapidity Density Distribution of Photons

Photons are produced from every phase of the fireball expansion, like from hard scattering to the decay of hadrons in heavy-ion collision experiment. Photons hardly interact with the medium. So when photons get thermalized, their mean free paths become same as the system size and they leave the system unaffected. Thus it is believed that the photons carry the information of the thermalized system at all stages of

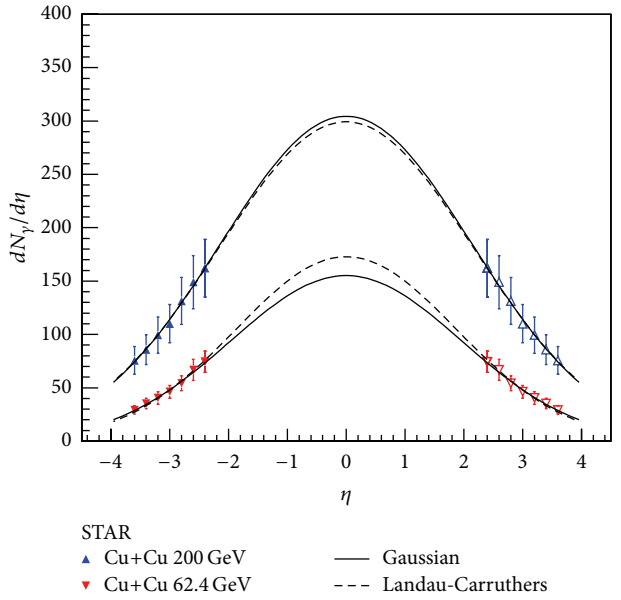

FIGURE 25: Photon multiplicity distributions of Cu+Cu collision system as a function pseudorapidity for the most central events for different collision energies.

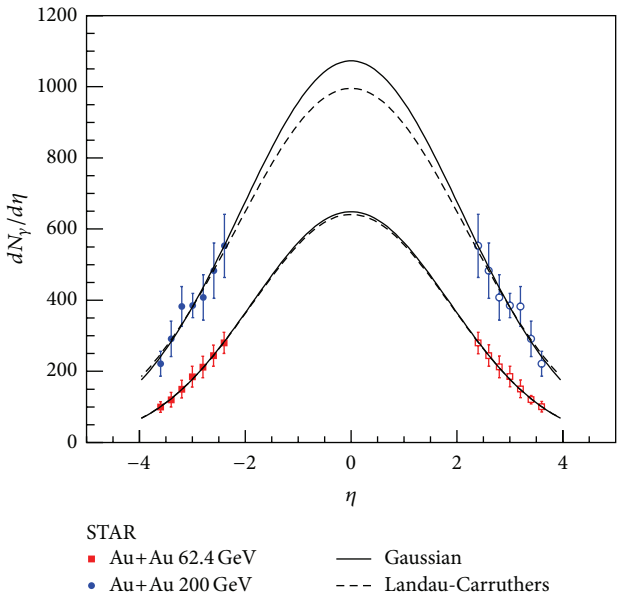

FIGURE 26: Photon multiplicity distributions of Au+Au collision system as a function pseudorapidity for the most central events for different collision energies.

the evolution of the produced fireball. Direct photons created from the QCD process are treated as golden probe to measure the thermodynamic parameters like initial temperature of the fireball. The inclusive photon spectra contain all photons including the photons produced from particle's decay, for example, π^0 and η^0. So photons can be used to estimate the degree of thermalization of the system. It is also proposed that as majority of photons are produced from π^0 decay, they can be used as a complementary measurement to the charged pion measurements. Photons can be used to study the anisotropic flow of the system. Photons can be used as a precursor for the measurement of pseudorapidity density distribution of charged particles. It is proposed that simultaneous measurement of charged particles with photons can be used in the search for Disoriented Chiral Condensate (DCC) [61–63]. Keeping the importance of measurement of photons in mind as a probe for QGP, we will be discussing the pseudorapidity distribution of photons.

In this review, the pseudorapidity density of photons for different collision systems and at different energies is discussed. Then the expansion hydrodynamics of photons are discussed by invoking Landau hydrodynamics along with its advanced forms. In the forward rapidity, longitudinal scaling of photons is discussed. At the end, the scaling of total measured photons as a function of $\langle N_{\text{part}} \rangle$ is discussed for two collision systems.

4.1. System Size and Energy Dependence of Photon Distributions ($dN_\gamma/d\eta$). The energy dependence of pseudorapidity distributions of photons is shown for Cu+Cu, Au+Au systems in Figures 25 and 26. In Figure 25, the pseudorapidity distribution of photons for Cu+Cu collisions at $\sqrt{s_{\text{NN}}}$ = 62.4 and 200 GeV is shown. In Figure 26, $dN_\gamma/d\eta$ for Au+Au collisions at $\sqrt{s_{\text{NN}}}$ = 62.4 and 200 GeV is shown. The Cu+Cu and Au+Au collision data are taken from STAR experiment at RHIC [65, 66]. The pseudorapidity distributions of photons of S+Au collision data at 19.3 GeV and Pb+Pb collisions at 17.6 GeV are shown in Figure 27. The S+Au collision data and Pb+Pb collision data are taken from [67] and [68], respectively. Data collected are at the forward rapidity. However, to get the photon distribution in the backward rapidities, a reflection of the data about the midrapidity is

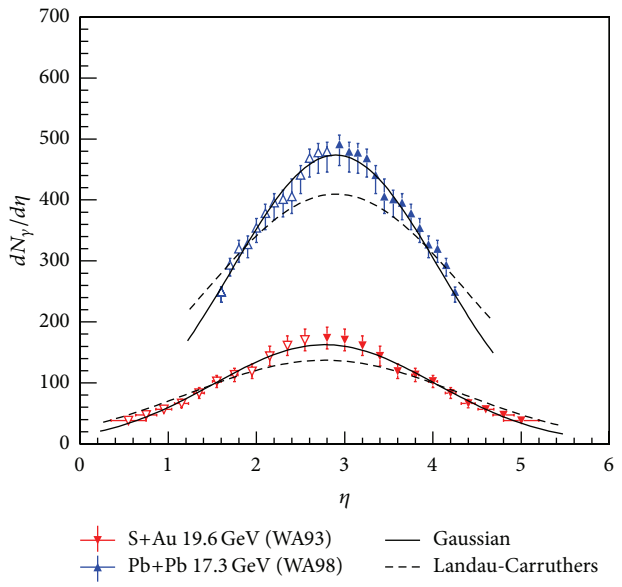

FIGURE 27: Photon multiplicity distributions of Pb+Pb collision system as a function pseudorapidity for the most central events for different collision energies.

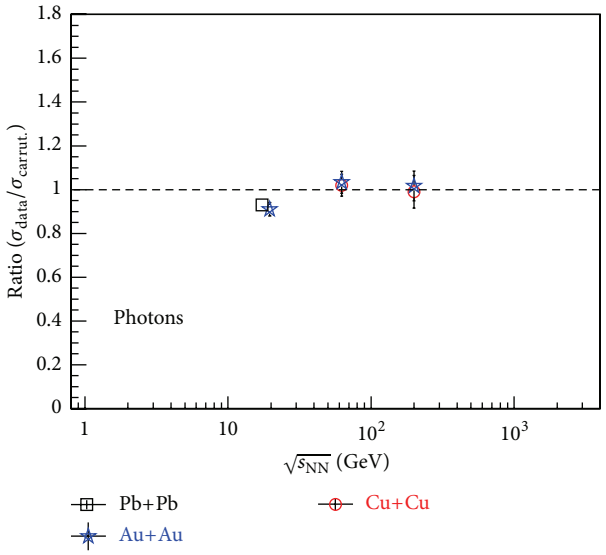

FIGURE 28: Ratio of the widths of the data and that obtained from the fitting of photon multiplicity distributions of different collision systems as a function of collision energy.

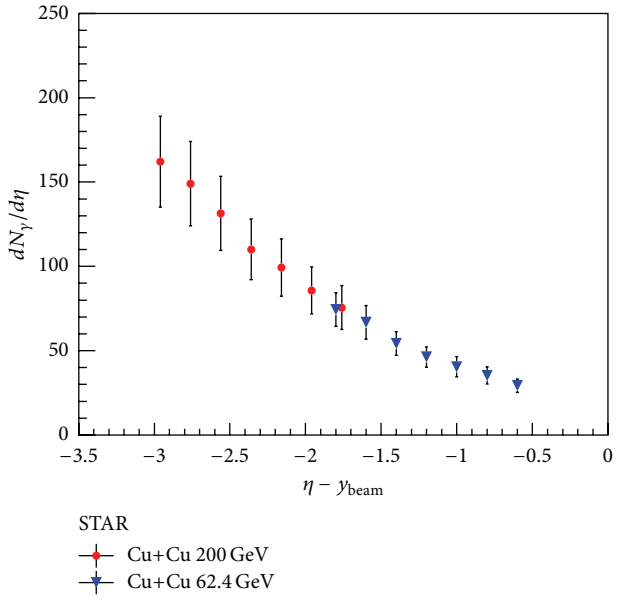

FIGURE 29: Photon multiplicity density normalized per participant pair for different energies, shown in one of the rest frames of the projectile.

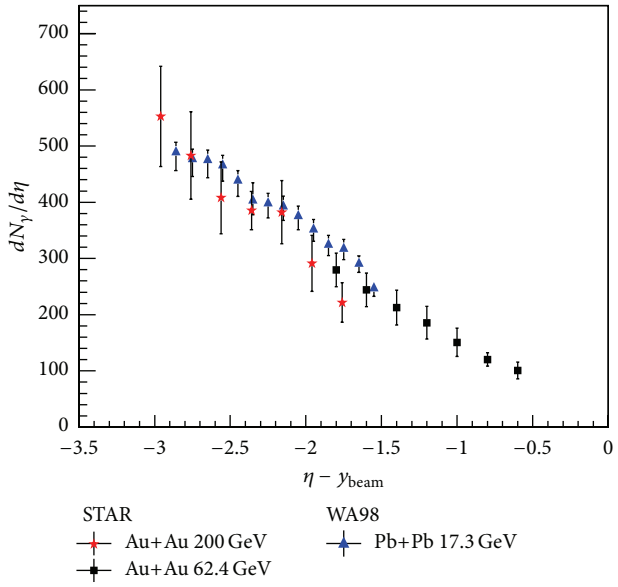

FIGURE 30: Photon multiplicity density normalized per participant pair for different energies shown in the projectile rest frame.

done assuming that the $dN_\gamma/d\eta$ is symmetric about $\eta = 0$ for collider experiments, for example, Cu+Cu and Au+Au collisions. For fixed target experiments, like S+Au and Pb+Pb, the reflection is carried out with respect to the η_{peak}. The open markers represent the mirror reflection of the data recorded by the detectors. The $dN_\gamma/d\eta$ distributions are fitted with a double Gaussian (6) and Landau-Carruthers functions (15) to understand the expansion dynamics of the system. To see the extent to which the Landau hydrodynamics is applicable to the system, the ratio of width of the $dN_\gamma/d\eta$ of data and the width obtained from Landau-Carruthers fitting is shown as a function of collision energies in Figure 28. It can be observed that at lower energy it deviates from 1, but at RHIC energy it agrees with Landau-Carruthers hydrodynamical model. At LHC energies, the fragmentation region will also be affected by the decayed photons generated from the gluonic sources in the midrapidity. Therefore, it would be interesting to have corresponding LHC data to look into the validity of Landau hydrodynamics for photons at forward rapidities.

4.2. Longitudinal Scaling of Photon. In the previous section, the longitudinal scaling of charged particles in the forward rapidities is discussed. Is this longitudinal scaling a global phenomenon of the heavy-ion collision or only specific to charged particle productions? To confirm this phenomenon, the longitudinal scaling of photons is studied separately for two different collision species. In Figure 29, the $dN_\gamma/d\eta$ as a function of η' for Cu+Cu collision data at $\sqrt{s_{NN}} = 62.4$ and 200 GeV are shown. In Figure 30, the $dN_\gamma/d\eta$ for Au+Au collisions at $\sqrt{s_{NN}} = 62.4$, 200 GeV and Pb+Pb collision data at beam energy 158 AGeV as a function of η' are shown. The $dN_\gamma/d\eta$ data are available for only small pseudorapidity coverage. Still, the nature of the $dN_\gamma/d\eta$ distribution as a function of η' shows the longitudinal scaling behaviour as consequences of limiting fragmentation. It is observed from Figures 29 and 30 that photon also shows the energy independent limiting fragmentation behaviour. It is seen that the limiting fragmentation of pions is the same as the photon and independent of centrality unlike charged hadrons. It is also reported in [66] that the limiting fragmentation behaviour of photons for $p + \overline{p}$ collisions at $\sqrt{s} = 540$ GeV is in close agreement with the measured photon yield in Au+Au collisions at $\sqrt{s_{NN}} = 62.4$ GeV unlike the charged particle results. Study from HIJING event generator indicates

that about 93–96% of measured photons are from π^0 decays. Hence, the centrality independent behaviour of photons is interpreted as indirect measure of meson limiting fragmentation. This contrasting behaviour of photon results of the limiting fragmentation with respect to charged hadrons may be due to nuclear remnants and baryon stopping. It indicates that mesons are not affected by baryon transport at forward rapidities [66]. The study of identified charged particles with photon results done in [66] clearly indicates that net-proton results violate the energy independent behaviour of limiting fragmentation: a clear indication of baryon-meson anomaly. The centrality and energy independence behaviour of mesons contrary to inclusive charged hadrons and identified baryons implies that baryon transport plays an important role in particle production at forward rapidities. It is argued that although the baryon stopping is different for different collision energies, the mesons are not affected by it. In the context of baryon junction picture, baryons would have shown the energy independent limiting fragmentation behaviour at forward rapidities, if they carry the valance quarks like the mesons produced from the valance quarks. This suggests that baryon number resides in a nonperturbative configuration of gluon fields rather in the valence quarks [66].

The longitudinal scaling behaviour observed for charged particles and photons ensures the universality of hypothesis of limiting fragmentation and puts forward many deeper questions about the actual processes behind it.

During the discussion of extended longitudinal scaling of charged particles, we have encountered that this is independent of energy but shows some dependence of collision geometry, that is, centrality. Then R_{PC} variable was adopted to deal with this issue. But in the limiting fragmentation of photons, it is found to be centrality independent [66]. But to see the consistency, we tried to do the same exercise for photons by evaluating the R_{PC} for different collision systems at different energies. The R_{PC} is defined as given in (4). For the RHIC energies, the peripheral events correspond to 30–40% centrality and central events correspond to 0–5% centrality. For WA98 experiment, 25–35% centrality and 0–5% events are considered as peripheral events and central events, respectively. In Figure 31, R_{PC} for Cu+Cu collision data at $\sqrt{s_{\mathrm{NN}}}$ = 62.4 and 200 GeV are shown as a function of η'. Similarly, in Figure 32, R_{PC} of Au+Au collision data at $\sqrt{s_{\mathrm{NN}}}$ = 62.4 and 200 GeV superimposed with Pb+Pb data at beam energy 158 AGeV are shown as a function of η'. The error bars shown in Figures 31 and 32 are for statistics only. We observe from Figures 31 and 32 that within error bars the R_{PC} is constant and equal to one as a function of η' irrespective of collision energies. This observation could be understood as follows. The rapidity (pseudorapidity) coverage of the detectors used for photon measurement is less than the beam rapidity and hence there is no contamination from the beam remnants and baryon stopping, which makes the R_{PC} go like one. This is also true for identified charged particle measurements as well. However, for the charged particle R_{PC}, the rising part for lower energies (shown in Figures 8 and 9) is due to the beam remnants and baryon stopping, as

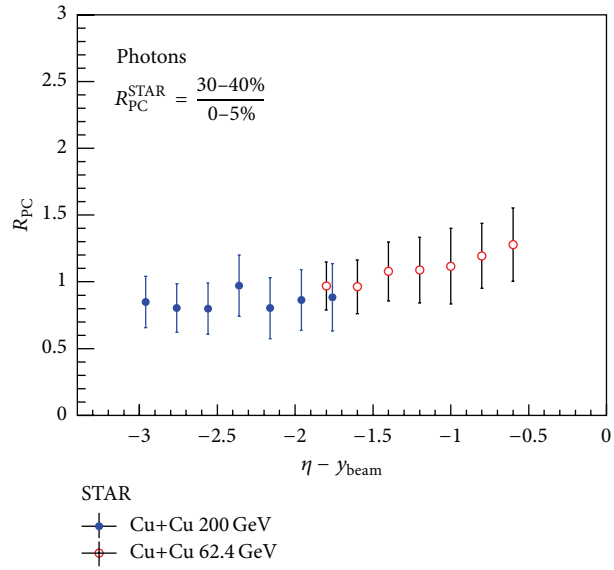

FIGURE 31: R_{PC} of photons as a function of $\eta' = \eta - y_{\mathrm{beam}}$ for Cu+Cu collisions for different energies.

the beam rapidity is less than the rapidity coverage of the detectors. It will be interesting to look into rapidity spectra of charged pions at lower energies like 19.6 GeV or below to rule out beam remnant or baryon stopping effects on this observation. In conclusion, the above discussions strengthen our argument that extended longitudinal scaling is a global phenomenon for charged particles as well as for photons produced in the heavy-ion collision experiments.

4.3. Scaling of N_γ^{total} with N_{part}. Like the scaling of total charged particles with N_{part}, the total photons normalized per participant pairs as a function of average participant pairs are shown for Cu+Cu and Au+Au collision systems at 62.4, 200 GeV in Figures 33 and 34, respectively. Both the data scale nicely and the normalized N_γ values increase with increase of collision energy. Note that N_γ is the value of total number of photons measured within the detector acceptance ($-3.7 < \eta < -2.3$) [65].

From Figures 33 and 34, we observed that N_γ scales with the collision centrality like charged particles.

5. Transverse Energy and Collision Cross Section

The transverse energy is one of the important global observables used to characterize the system formed in heavy-ion collisions at extreme conditions of temperature and energy density, where the formation of Quark-Gluon Plasma (QGP) is expected. The transverse energy (E_T) is the energy produced transverse to the beam direction and is closely

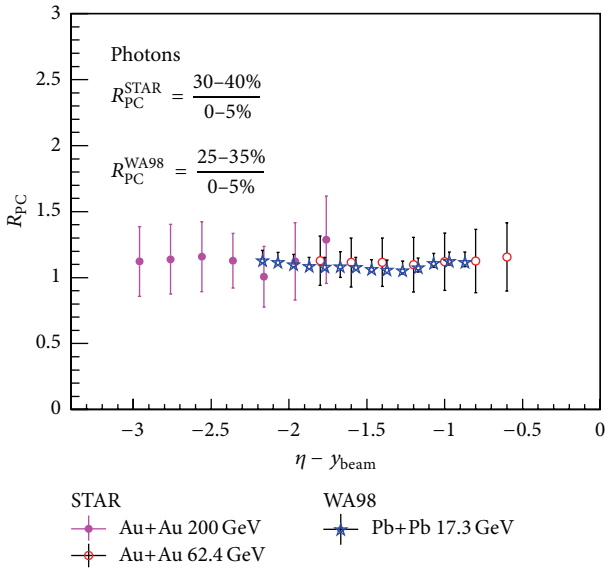

FIGURE 32: R_{PC} of photons as a function of $\eta' = \eta - y_{beam}$ for Au+Au collisions for different energies.

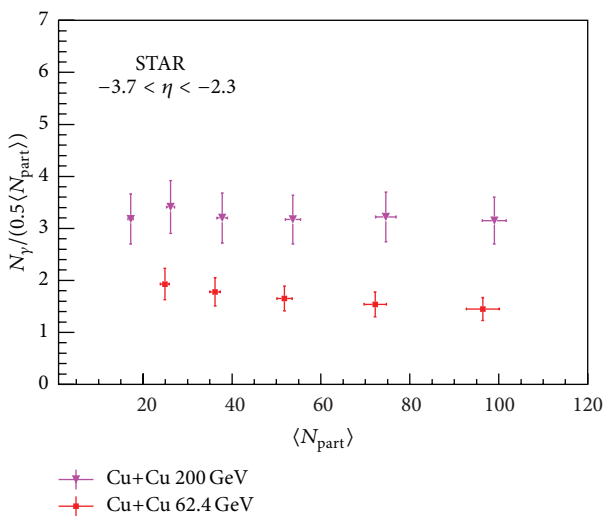

FIGURE 33: N_γ normalized per participant pair as a function of N_{part} for Cu+Cu collisions.

related to the collision geometry. E_T is an event-by-event variable defined as

$$E_T = \sum_i E_i \sin\theta_i, \qquad \frac{dE_T(\eta)}{d\eta} = \sin\theta(\eta)\frac{dE(\eta)}{d\eta}. \tag{25}$$

The sum is taken over all particles produced in an event within the detector acceptance. E_i and θ_i are the energy and polar angle of the final state particles. The energy of the individual particle can be determined by knowing their momenta and particle identification using tracking detectors and/or the total energy deposited in a calorimeter. The source of transverse energy production could be "soft" multiparticle production and/or the "hard" scattering jets, depending on

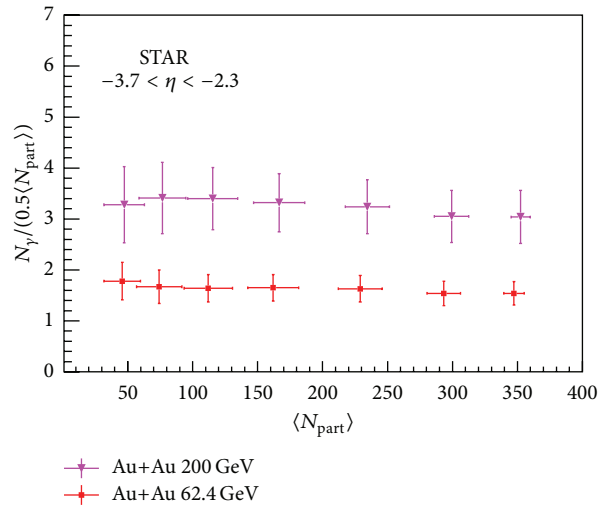

FIGURE 34: N_γ normalized per participant pair as a function of N_{part} for Au+Au collisions.

the collision energy. The transverse energy distribution is related to the multiplicity distribution by

$$\frac{dE_T}{d\eta} \sim \langle p_T\rangle \times \frac{dN}{d\eta}. \tag{26}$$

To probe the early stages of the produced fireball, it is ideal to take transverse observables like E_T, p_T, and so forth. This is because, before the collision of two nuclei, the longitudinal phase space is filled by the beam particles whereas the transverse phase space is empty. The E_T is produced due to the initial scattering of the partonic constituents of the incoming nuclei and also by the rescattering among the produced partons and hadrons [69, 70]. The E_T production tells about the explosiveness of the interaction. Additionally, in the framework of boost-invariant hydrodynamics, the measurement of E_T helps in the quantitative estimation of the initial energy density produced in the interaction [2]. A comparison of this initial energy density with that of estimated by the lattice QCD (lQCD) calculations gives indication of a possible formation of QGP in the corresponding heavy-ion interactions [3]. However, there are several competing processes to make a difference between the initially generated and finally observed E_T. In an ideal case, if the fireball of the produced quanta, namely, the partons or the hadrons depending on the case, break apart instantaneously without significant interactions, the observed transverse energy per unit rapidity dE_T/dy will be the same as generated initially. On the other hand, if the system interacts very strongly achieving an early thermal equilibrium, which is maintained though out the system expansion, dE_T/dy would decrease significantly due to the longitudinal work done by the hydrodynamic pressure [71, 72]. This decrease may however be moderated by the build-up of transverse hydrodynamic flow, which increases E_T [73]. At higher collision energies, the difference between initially generated and finally observed E_T may be reduced because of the gluon saturation in the wave function of the colliding heavy nuclei. This delays the onset of

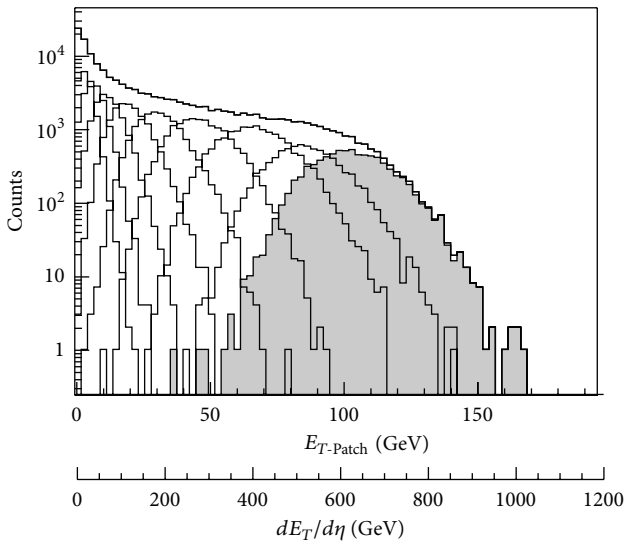

FIGURE 35: The midrapidity ($0 < \eta < 1$) minimum bias distribution of total transverse energy along with distributions for different centrality bins for $\sqrt{s_{\mathrm{NN}}} = 200$ GeV, as is measured by the STAR experiment at RHIC. The shaded area corresponds to the 5% most central bin. The main axis scale corresponds to the E_T measured in the detector acceptance and the bottom axis is corrected to represent the extrapolation to full azimuthal acceptance. The figure demonstrates the use of E_T distribution for estimation of collision centrality. The figure is taken from [64].

hydrodynamic flow and hence reduces the effective pressure, which decides the above difference [74].

The collision centralities can be estimated by using the minimum bias E_T distribution in a way it is done using the charged particle minimum bias distribution. This is shown in Figure 35. The shaded area in the figure corresponds to the most central (0–5%) collisions having the highest transverse energy. This corresponds to the 5% of the total cross section. Different centralities are defined by the percentages of total cross sections and are shown in the same figure. Each centrality class follows a Gaussian type of distribution with different mean and variance following the central limit theorem. The lower edge of the minimum bias distribution shows a peak, which corresponds to the most peripheral collisions. For the most central collisions corresponding to largest values of E_T, the shape of the distribution is mainly governed by the statistical fluctuations and the experimental acceptance. For larger acceptances, the fall-off with increasing E_T is very sharp [75].

Reference [75] gives a very interesting account of addressing a fundamental question like if E_T or the multiplicity is primary. In other words, whether E_T production is primary, followed by fragmentation to final state particles, or whether E_T is a random product of the particle multiplicity and the p_T distribution. The method as discussed in the above report is as follows. If one assumes that the E_T production is a result of the creation of the particles according to the semi-inclusive multiplicity distribution followed by the random assignment of transverse momentum to each particle in accordance with the single-particle semi-inclusive p_T distribution, the process could be described by the equation

$$\frac{d\sigma}{dE_T} = \sigma \sum_{n=1}^{n_{\max}} f_{\mathrm{NBD}}\left(n, \frac{1}{k}, \mu\right) f_{\Gamma}\left(E_T, np, b\right), \tag{27}$$

where the multiplicity distribution in $A + A$ collisions is represented by a Negative Binomial Distribution (NBD), $f_{\mathrm{NBD}}(n, 1/k, \mu)$ [77–79]. The E_T distribution for n particles in the final state is represented by a Gamma function, $f_{\Gamma}(E_T, np, b)$, where p and b are the parameters of the E_T distribution for a single particle [80]. The details of the NBD and Gamma distributions with their properties are given in the Appendix. If we assume that the E_T spectra for individual particles are independent of each other and in addition they are also independent of the multiplicity n, then the E_T spectrum for n particles is the nth convolution of the single particle spectrum. As one finds difficulty in the convergence of fits to (27), NBD was restricted to Poisson by fixing $1/k = 0$, which in turn makes the convergence easier. If one assumes a simpler proportionality between E_T and n, so the number of particles in an event n with transverse energy E_T are related by $n = E_T/\langle p_T \rangle$ (the nearest integer). The plot of $\langle E_T \rangle d\sigma/dE_T$ in barn as a function of $E_T/\langle E_T \rangle$ is fitted by the function given by (26) [75] and to the NBD given by

$$\frac{d\sigma}{dE_T} = \sigma f_{\mathrm{NBD}}\left(\frac{E_T}{\langle p_T \rangle}, \frac{1}{k}, \mu\right). \tag{28}$$

Note that the above NBD is now modified because of the simple relationship of E_T and the multiplicity n, given by (26). It is observed that the trend of the data leads to a better fit of single-Gamma distribution at higher values of E_T compared to NBD and the reverse at lower values of E_T. Usually fitting functions with more number of parameters give flexibility to the fitting leading to a better fit. However, in this case, complicated functions like (27) with more number of parameters give worse fit compared to simpler functions like (28). Single-Gamma distribution fitting to the above distribution is better than the other two functions. If multiplicity were the primary quantity compared to transverse energy, which leads to the form of (27) and (28), then one would expect these equations to fit better than the single-Gamma distribution. It is interesting and compelling to speculate on the implications of these results for a detailed relationship of multiplicity with transverse energy and the effect of hadronization. However, it remains as an open question to be addressed by more controlled experiments.

6. Collision Energy Dependence of Transverse Energy

Figure 36 shows the collision energy dependence of $(1/(N_{\mathrm{part}}/2))(dE_T/d\eta)$ for central collisions at midrapidity. A logarithmic growth of transverse energy up to the top RHIC energy underestimates the LHC measurement, which is better described by a power-law fit. However, the latter overestimates the low energy measurements. A hybrid function, which is a combination of logarithmic and power

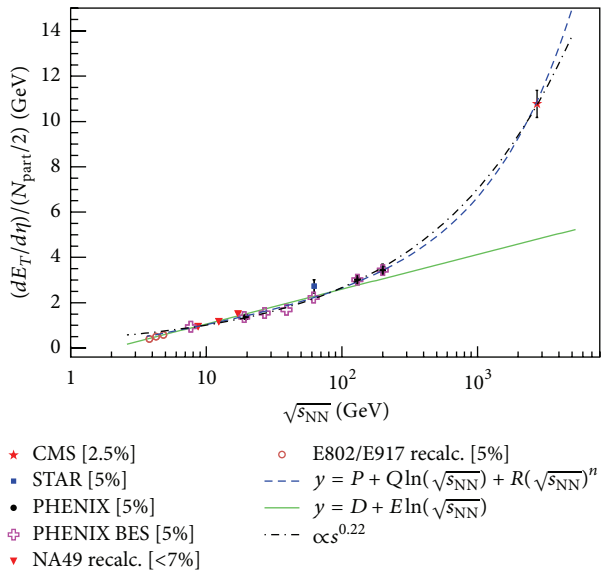

FIGURE 36: Collision energy dependence of midrapidity $(1/(N_{part}/2))(dE_T/d\eta)$. Shown are different phenomenological fitting functions to explain the transverse energy production.

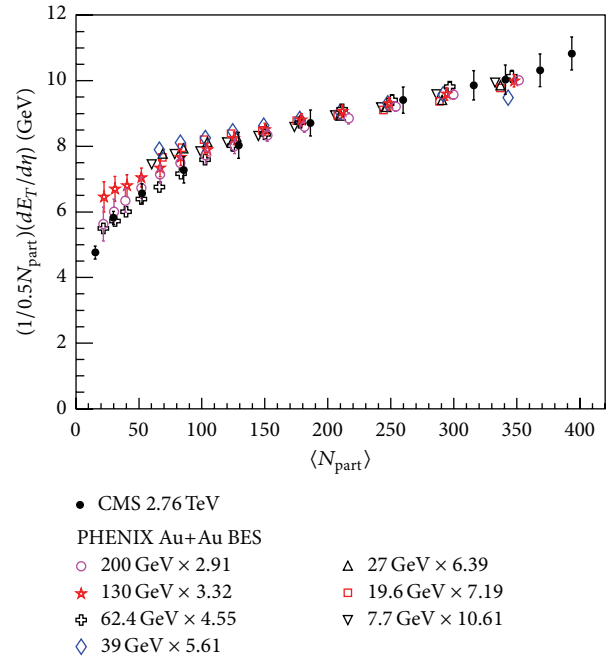

FIGURE 37: Centrality dependent participant pair-normalized $dE_T/d\eta$ at midrapidity.

law, motivated by midrapidity gluonic source and a fragmentation source, seems to explain the data for wide range of energies starting from few GeV to TeV [29, 43, 51]. $(1/(N_{part}/2))(dE_T/d\eta)$ increases by a factor of 3.07 from $\sqrt{s_{NN}}$ = 200 GeV to 2.76 TeV. The CMS experiment reports the estimation of $dE_T/d\eta = 2007 \pm 100$ GeV and $dN_{ch}/d\eta = 1612 \pm 55$ for top 5% central Pb+Pb collisions at 2.76 TeV [15, 28]. Division of both leads to transverse energy per charged particle of 1.25 ± 0.08 GeV at $\sqrt{s_{NN}}$ = 2.76 TeV, for top 5% central Pb+Pb collisions, which is almost 42% higher than its corresponding value at top RHIC energy (0.88 ± 0.07 GeV). Recently, a model of effective energy [47, 60] has been applied [53] to the N_{part} and $\sqrt{s_{NN}}$ dependencies of transverse energy midrapidity density. It is shown that the E_T data are well described from a few GeV at GSI up to a few TeV at the LHC pointing to the centrality data to be complementary to the head-on collision data, as already found for the midrapidity pseudorapidity nuclear measurements.

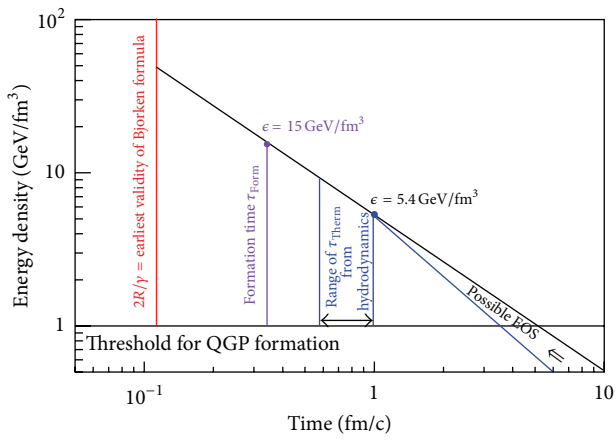

FIGURE 38: Schematic diagram of the time and energy density scales derived through the Bjorken picture [76].

7. Centrality Dependence of Transverse Energy

Figure 37 shows the centrality dependence of $(1/(N_{part}/2))(dE_T/d\eta)$ at midrapidity. Various lower energy measurements are multiplied with some numbers to look into the similarity in the shape at higher energies. Except extreme peripheral events, within experimental uncertainties the centrality shows a universal shape for all energies. The value of $(1/(N_{part}/2))(dE_T/d\eta)$ shows a monotonic increase with collision centrality.

One of the goals of heavy-ion collision experiments is to create QGP in the laboratory and a prerequisite of this is to ensure that sufficiently large energy density has been produced in the heavy-ion collisions. To ensure this, the estimation of the initial energy density through the measurement of the final state multiplicity and transverse energy is done through Bjorken hydrodynamic model. Numerical simulations on lattice [3, 81, 82] give a lower bound for the initial energy density for the formation of a Quark-Gluon Plasma, which is of the order of 1 GeV/fm^3 [3]. A comparison of the estimated energy density from Bjorken model may establish the possible formation of QGP in heavy-ion collisions at a given collision energy. A schematic diagram of energy density as a function of fireball evolution time is given in Figure 38. In general one can think of three different energy density estimates and two different time scales:

(1) The peak *general energy density*, which is achieved when the incoming nuclei overlap with each other.

(2) The peak *formed energy density*, which involves the produced particles at a proper time τ_{form}.

(3) The peak *thermalized energy density*, present at proper time τ_{therm}, when local thermal equilibrium is first achieved, assuming that this occurs.

In this review we will restrict ourselves to the discussion on the formed energy density estimated through Bjorken boost invariant hydrodynamics. However, for a detailed discussion one can refer to [76].

8. Bjorken Hydrodynamics and Initial Energy Density

The energy density in general is defined as the ratio of total mass-energy within some region of space and the volume of that region, as seen at some instant of time in some Lorentz frame. As discussed in [76], this definition is not satisfactory, as one can easily raise any energy density by viewing the system from a different frame of reference. For example, a gold or lead nucleus with constant energy density ρ_0, when viewed in a boosted frame, will appear to have energy density $\gamma^2\rho_0$, where γ is the value of the Lorentz boost factor. In a region having total momentum zero, one can meaningfully calculate the energy density as ratio of mass-energy and volume. Considering symmetric heavy-ion collisions $(A+A)$ in collider experiments, with an overlapping of two nuclei, viewed in the center of momentum frame, the total energy density in the overlapping region is given by $\langle\epsilon\rangle = 2\rho_0\gamma^2$. If we take the normal nuclear matter density, $\rho_0 = 0.14\,\text{GeV/fm}^3$, for a nucleus at rest and $\gamma = 106$ at $\sqrt{s_{\text{NN}}} = 200\,\text{GeV}$, then the general energy density is $\langle\epsilon\rangle = 3150\,\text{GeV/fm}^3$ at RHIC. For LHC $\sqrt{s_{\text{NN}}} = 2.76\,\text{TeV}$ Pb+Pb collisions, $\gamma = 1471.2$, which leads to $\langle\epsilon\rangle = 606053\,\text{GeV/fm}^3$. As these numbers are spectacularly high, when compared to the lQCD predicted value of $1\,\text{GeV/fm}^3$ energy density as a condition for the formation of a QGP phase seems to be absurd. Hence, our interest would be to consider the energy density of the produced particles in order to infer about the possible formation of a QGP phase. This is done through the measurement of transverse energy at midrapidity and further the estimation of initial energy density in Bjorken hydrodynamic model.

In the framework of Bjorken boost invariant hydrodynamic model, in any frame where the two incoming nuclei have very high energies, the region when/where the nuclei overlap will be very thin in the longitudinal direction and very short in duration. In this scenario, it is fair to describe that all produced particles are created at the same time and radiated out from a thin disk. This is the Bjorken hydrodynamic picture of nucleus-nucleus collision [2].

Once the Lorentz contracted beam "pancakes" recede after their initial overlap, the region between them is occupied by secondaries at intermediate rapidities. We can calculate the local energy densities of these created particles, if we assume the secondaries are formed at some proper time τ_{form}.

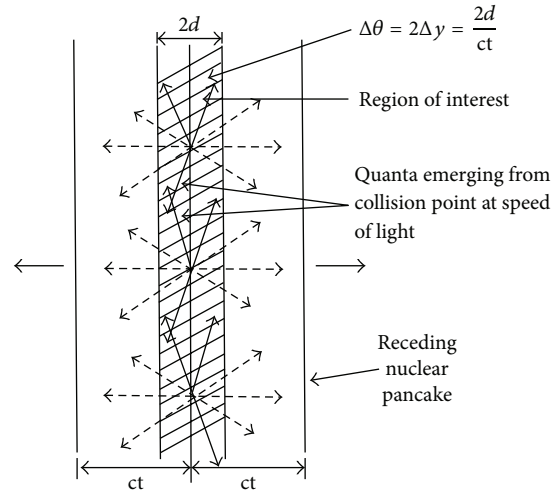

Figure 39: Geometry for the initial state of centrally produced plasma in nucleus-nucleus collisions. This picture is valid in any frame in which the incoming nuclei have very high energies and so, are Lorentz contracted. The figure is taken from [2].

Our region of interest, in any frame, will be a slab perpendicular to the beam direction, with longitudinal thickness dz, with one face of the "source" plane in this frame, and the transverse overlap area A. The region described here corresponds to half the shaded region shown in Figure 39. Since $\beta_\parallel \simeq 0$ for particles near the source location, this is an appropriate region over which we can calculate a meaningful energy density. At time $t = \tau_{\text{form}}$, this volume will contain all the (now-formed) particles with longitudinal velocities $0 \le \beta_\parallel \le dz/\tau_{\text{form}}$ (since we assume particles cannot scatter before they are formed!). Then we can write this number of particles as $dN = (dz/\tau_{\text{form}})(dN/d\beta_\parallel)$, or equivalently $dN = (dz/\tau_{\text{form}})(dN/dy)$, where y is longitudinal rapidity, since $dy = d\beta_\parallel$ at $y = \beta_\parallel = 0$. If these particles have an average total energy $\langle m_T\rangle$ in this frame ($E = m_T$ for particles with no longitudinal velocity), then the total energy divided by the total volume of the slab at $t = \tau_{\text{form}}$ is

$$\begin{aligned}\left\langle\epsilon\left(\tau_{\text{form}}\right)\right\rangle &= \frac{dN\langle m_T\rangle}{dzA} \\ &= \frac{dN\left(\tau_{\text{form}}\right)}{dy}\frac{\langle m_T\rangle}{\tau_{\text{form}}A} \\ &= \frac{1}{\tau_{\text{form}}A}\frac{dE_T\left(\tau_{\text{form}}\right)}{dy},\end{aligned} \tag{29}$$

where we have equated $dE_T/dy = \langle m_T\rangle(dN/dy) \approx \langle m_T\rangle (3/2)(dN_{\text{ch}}/dy)$ and emphasized that (29) is true for the transverse energy density present at time $t = \tau_{\text{form}}$. The factor 3/2 compensates for the neutral particles.

Equation (29) is referred to as *Bjorken energy density*, ϵ_{Bj}. It is a valid measure of peak energy density in created particles, on very general grounds and in all frames, as long as two conditions are satisfied: (1) a finite formation time τ_{form} can meaningfully be defined for the created secondaries; and (2) the thickness/"crossing time" of the source disk is small

compared to τ_{form}, that is, $\tau_{\text{form}} \gg 2R/\gamma$. Here R is the rest-frame radius of the nucleus and γ is the Lorentz factor. In particular, the validity of (29) is completely independent of the shape of the $dE_T(\tau_{\text{form}})/dy$ distribution to the extent that $\beta_{\parallel}$ is infinitesimally small in a comoving frame; a plateau in dE_T/dy is not required. For practical purposes at RHIC, we will consider condition (2) above to be satisfied as long as $\tau_{\text{form}} > 2R/\gamma$ is true.

Historically, ϵ_{Bj} has been calculated using the final state dE_T/dy and simply inserting a nominal value of 1 fm/c for τ_{form}. In addition, fixed target experiments have been using $dE_T/d\eta$ as an estimate for dE_T/dy, which is a good approximation for these experiments. For collider experiments, a correction is made for the Jacobian $dy/d\eta$: $(\sqrt{1 - m^2/\langle m_T\rangle^2}(dN/dy) = J(dN/dy) = dN/d\eta)$. However, we cannot take ϵ_{Bj} as an exact estimate of energy density without some justification for the value of 1 fm/c taken for τ_{form}. Hence, we term it as $\epsilon_{\text{Bj}}^{\text{Nominal}}$. An indication of potential problems with this choice arises immediately when considering AGS Au+Au and SPS Pb+Pb collisions, where the center of mass "crossing times" $2R/\gamma$ are 5.3 fm/c and 1.6 fm/c, respectively, which implies that this choice for $\tau_{\text{form}} = 1$ fm/c actually violates the validity condition $\tau_{\text{form}} > 2R/\gamma$ we set for the use of (29). So we will deprecate the use of $\epsilon_{\text{Bj}}^{\text{Nominal}}$ as a quantitative estimate of actual produced energy density and instead treat it only as a compact way of comparing $dE_T/d\eta$ measurements across different systems, centralities, and beam energies.

The Bjorken energy density obtained in this framework is given by

$$\epsilon_{\text{Bj}} = \frac{dE_T}{dy}\frac{1}{\tau_0 \pi R^2} \tag{30}$$

$$= \frac{dE_T}{d\eta} J(y,\eta)\frac{1}{\tau_0 \pi R^2} \tag{31}$$

$$\simeq \langle m_T\rangle \frac{3}{2}\frac{dN_{\text{ch}}}{dy}\frac{1}{\tau_0 \pi R^2}, \tag{32}$$

where τ_0 is the formation time, usually assumed to be 1 fm/c, and πR^2 is the transverse overlap area of the colliding nuclei. The formation time is usually estimated from model calculations and has been a matter of debate. There are different ways to estimate the transverse overlap area. It goes like $N_{\text{part}}^{2/3}$ in an approach which accounts for only the common area of colliding nucleons but not the nuclei (chosen by STAR). In this approach, the transverse overlap area $F = \pi R^2$, where $R = R_0 A^{1/3}$. When we replace A with the number of participants by $A = N_{\text{part}}/2$ [8], F becomes

$$F = \pi R_0^2 \left(\frac{N_{\text{part}}}{2}\right)^{2/3}. \tag{33}$$

In the other approach (adopted by PHENIX) [83], the transverse overlap area of the colliding species, F, is estimated in the following way. The Woods-Saxon parametrization for the nuclear density profile is given by

$$\rho(r) = \frac{1}{\left(1 + e^{(r-r_n)/d}\right)}, \tag{34}$$

where $\rho(r)$ is the nuclear density profile, r_n is the nuclear radius, and d is a diffuseness parameter. Based on the measurements of electron scattering from Au nuclei [84, 85], r_n is set to (6.38 ± 0.27) fm and d to (0.54 ± 0.01) fm. A Monte Carlo Glauber model with $F \sim \sigma_x \sigma_y$ (where σ_x and σ_y are the widths of x and y position distributions of the participating nucleons in the transverse plane) is used to estimate the transverse overlap area of two colliding nuclei. In this approach, F is the transverse overlap area of two colliding nuclei, not the participating nucleons. The normalization to πR^2, where R is the sum of r_n and d parameters in the Woods-Saxon parametrization (given by (34)), is done for most central collisions at the impact parameter $b = 0$.

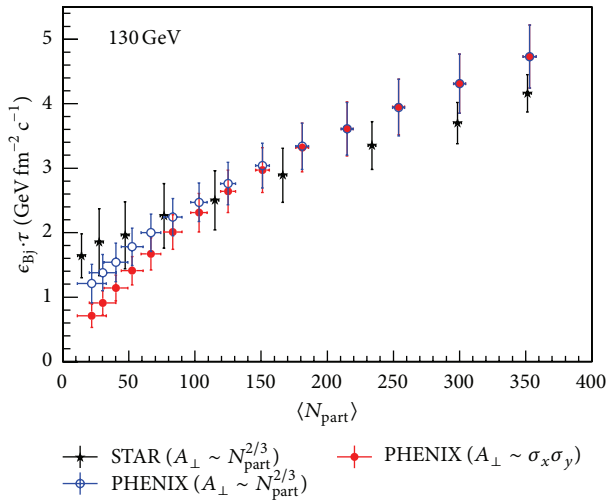

FIGURE 40: The Bjorken energy density versus N_{part} using different estimates of the transverse overlap area at $\sqrt{s_{\text{NN}}} = 130$ GeV. The figure is taken from [43].

The results obtained in these two methods, as shown in Figure 40, are different only in the peripheral bins. The results obtained by STAR agree with PHENIX results within systematic errors. However, STAR data show a smaller rate of increase of the energy density with N_{part}. As can be seen from the figure, the results agree rather well within uncertainties for central collisions, where we expect a deconfinement of quarks and gluons to take place.

In the estimation of $\epsilon_{\text{Bj}} \cdot \tau$, one uses the energy and rapidity dependent Jacobian factor, $J(y,\eta)$, for the conversion of pseudorapidity to rapidity phase space. The value of the Jacobian is smaller at higher energies, as the average transverse momentum of particles increases with beam energy. STAR collaboration uses a factor of 1.18 for $\eta \rightarrow y$-phase space conversion, as compared to 1.25 used by PHENIX [27, 83] for the estimation of Bjorken energy density at 200 GeV. The values of ϵ_{Bj} for Au+Au collisions at $\sqrt{s_{\text{NN}}} = 19.6$, 130 [27, 83], and 200 GeV [64] are 2.2 ± 0.2, 4.7 ± 0.5, and $4.9 \pm$

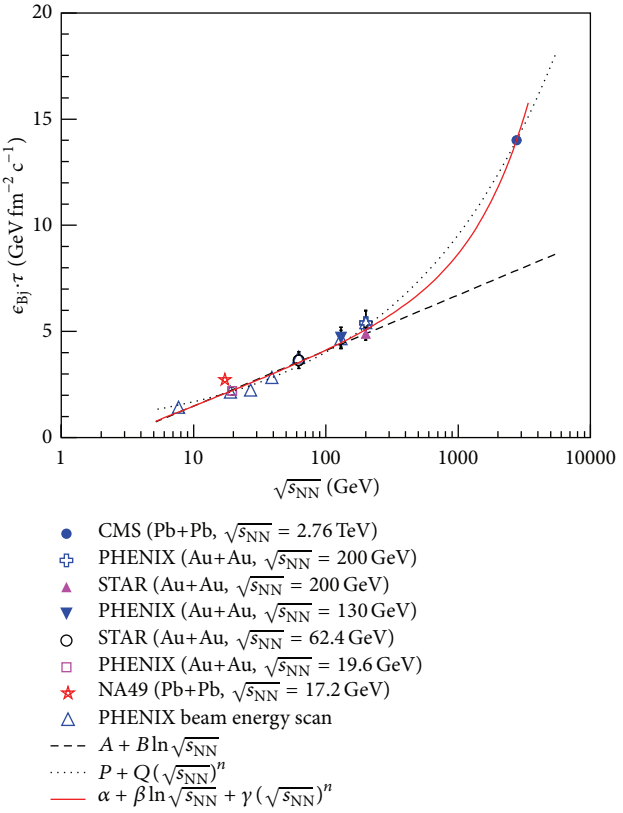

FIGURE 41: The excitation function of $\epsilon_{Bj} \cdot \tau$ [GeV fm^{-2} c^{-1}]. Logarithmic prediction fails to explain the LHC data. Shown are different phenomenological data driven fitting functions to describe the observable as a function of collision energy.

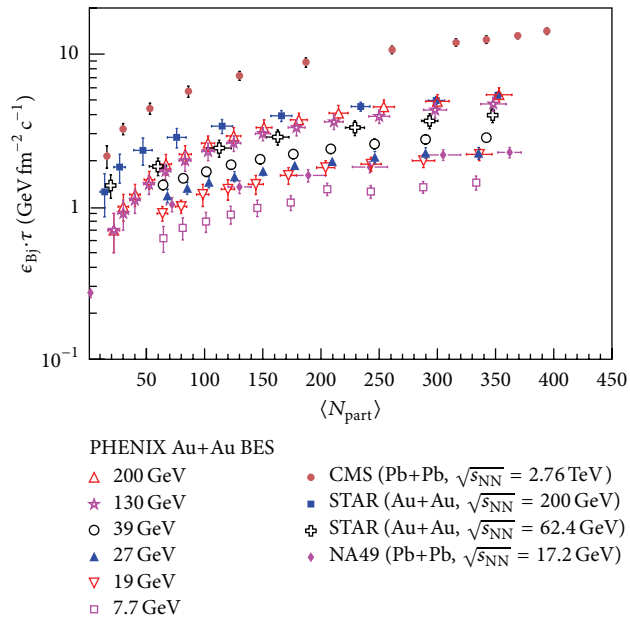

FIGURE 42: The N_{part} dependence of the product of the Bjorken energy density and the formation time ($\epsilon_{Bj} \cdot \tau$) for Au+Au system at different energies at RHIC compared to Pb+Pb collisions at LHC.

0.3 GeV/fm^3 (5.4 ± 0.6 GeV/fm^3, PHENIX), respectively. Compared to this, ϵ_{Bj} at SPS for Pb+Pb collisions at $\sqrt{s_{NN}}$ = 17.2 GeV is found to be 3.2 GeV/fm^3 [86]. This value of ϵ_{Bj} is much higher than the same for Au+Au collisions at the SPS-like energy; that is, $\sqrt{s_{NN}}$ = 19.6 GeV at RHIC. The CMS collaboration has estimated ϵ_{Bj} = 14 GeV/fm^3 with transverse overlap area of $A = \pi \times (7\,\text{fm}^2)$ and $J(y, \eta) = 1.09$ for top 5% central Pb+Pb collisions at $\sqrt{s_{NN}}$ = 2.76 TeV [28]. As all these estimations assume the same formation time of 1 fm/c, there is an overestimation of ϵ_{Bj} at SPS. In any case these energy densities are significantly larger than the energy density (~1 GeV/fm^3) predicted by lattice QCD calculations [3] for a transition to a deconfined Quark-Gluon Plasma phase. Following the deconfinement transition, there is a hydrodynamic expansion. Subsequently local equilibrium is achieved at $\tau_0 \sim 1$ fm/c. This picture is indeed valid, if we compare the RHIC data for elliptic flow to the hydrodynamic calculations [87–89].

Taking all ϵ_{Bj} measured for heavy-ion collisions at different energies and colliding species, we show $\epsilon_{Bj} \cdot \tau$ as a function of collision energy in Figure 41. This is done using (32). The dashed line is a logarithmic fit. The logarithmic extrapolation of $\epsilon_{Bj} \cdot \tau$ for Pb+Pb collisions at $\sqrt{s_{NN}}$ = 2.76 TeV at LHC is around 7.17 GeV fm^{-2} c^{-1}. However, the experimental estimation gives a value of $\epsilon_{Bj} \cdot \tau$ = 14 GeV fm^{-2} c^{-1}, showing almost 50% underestimation by the logarithmic trend of the data. On the other hand, a hybrid fitting function, which is a combination of logarithmic and power law functions in center of mass energy, describes the data from few GeV to TeV energies [29, 43, 51]. Fitting a power law function overestimates the low energy measurements. It should be noted that the formation time at LHC will be much less than 1 fm. The above value sets a lower bound to the initial energy density formed at LHC. Going from top RHIC energy to LHC 2.76 TeV, $\epsilon_{Bj} \cdot \tau$ increases almost 3 times. Figure 42 shows the estimations of the product of the Bjorken energy density and the formation time ($\epsilon_{Bj} \cdot \tau$) as a function of the centrality of the collision in terms of N_{part}. As expected there is a monotonic increase in $\epsilon_{Bj} \cdot \tau$ with increasing centrality of the collision.

While comparing the results from different experiments, related to the initial energy density, one needs to take care of the following factors: (i) value of the formation time taken into the calculations, (ii) the procedure of estimation of the transverse overlap area, and (iii) the value of the Jacobian used to transform η to y phase space.

8.1. The Formation Time. Is it possible to justify a better estimate for τ_{form}? From general quantum mechanical arguments, in a frame where its motion is entirely transverse, a particle of energy m_T can be considered to have "formed"

after a time $t = \hbar/m_T$. To estimate the average transverse mass, we can use the final state $dE_T/d\eta$ to estimate $dE_T(\tau_{\rm form})/dy$ and, correspondingly, use the final state $dN/d\eta$ as an estimate for $dN(\tau_{\rm form})/dy$ to obtain

$$\langle m_T \rangle = \frac{dE_T\left(\tau_{\rm form}\right)/dy}{dN\left(\tau_{\rm form}\right)/dy} \simeq \frac{dE_T/d\eta}{dN/d\eta} \quad \text{(Final state)}. \quad (35)$$

It has been observed experimentally that the ratio of final state transverse energy density to charge particle density, each per unit pseudorapidity, is constant at about 0.85 GeV for central Au+Au collisions at top RHIC energy. This value is constant for a wide range of centrality and shows a very little change with beam energy, decreasing to 0.7 GeV, when $\sqrt{s_{\rm NN}}$ is decreased by a order of magnitude down to 19.6 GeV. However, at LHC, its observed value is 1.25 ± 0.08 GeV, which will be discussed in the next section. If we approximate $dN_{\rm ch}/d\eta = (2/3)dN/d\eta$ in the final state, then (35) would imply $\langle m_T \rangle \simeq 0.57$ GeV and corresponding $\tau_{\rm form} \simeq 0.35$ fm/c, a value shorter than the "nominal" 1 fm/c but long enough to satisfy the given validity condition $\tau_{\rm form} > 2R/\gamma$ at RHIC. With $R = 7$ fm for Au+Au collisions and Lorentz factor $\gamma = \sqrt{s_{\rm NN}}/2m_p = 106.6$, at $\sqrt{s_{\rm NN}} = 200$ GeV, $2R/\gamma = 0.13$ fm/c. For LHC, at $\sqrt{s_{\rm NN}} = 2.76$ TeV, the observed $\langle p_T \rangle \sim 0.678$ GeV for Pb+Pb collisions [96]. Taking pion mass, one gets $\langle m_T \rangle \sim 0.81$ GeV, which leads to $\tau_{\rm form} \simeq 0.25$ fm/c. For Pb+Pb collisions at $\sqrt{s_{\rm NN}} = 2.76$ TeV, taking $R = 7.1$ fm, Lorentz factor, $\gamma = 1471.22$, we get $2R/\gamma = 0.01$ fm/c. Hence, the condition of $\tau_{\rm form} > 2R/\gamma$ is also satisfied at LHC. Similar numbers for the formation time at RHIC and LHC are also obtained in a calculation taking pions as dominant final state particles [97].

It is worth noting that the value of energy density obtained by (29) represents a conservative lower limit on the actual $\langle \epsilon(\tau_{\rm form}) \rangle$ achieved at RHIC. This follows from two observations: (1) The final state measured $dE_T/d\eta$ is a solid lower limit on the $dE_T(\tau_{\rm form})/dy$ present at formation time. (2) The final state ratio $(dE_T/d\eta)/(dN/d\eta)$ is a good lower limit on $\langle m_T \rangle$ at formation time and so yields a good upper limit on $\tau_{\rm form}$. The justification of these statements could be realized as follows.

There are several known mechanisms that will decrease dE_T/dy as the collision system evolves after the initial particle formation, while no mechanism is known that can cause it to increase (for $y = 0$, at least). Therefore, its final state value should be a solid lower limit on its value at any earlier time. A list of mechanisms through which dE_T/dy will decrease after $t = \tau_{\rm form}$ includes the following: (i) The initially formed secondaries in any local transverse "slab" will, in a comoving frame, have all their energy in transverse motion and none in longitudinal motion; if they start to collide and thermalize, at least some of their E_T will be converted to longitudinal modes in the local frame. (ii) Should near local thermal equilibrium be obtained while the system's expansion is still primarily longitudinal, then each local fluid element will lose internal energy through pdV work and so its E_T will decrease. (iii) If there are pressure gradients during a longitudinal hydrodynamic expansion then some fluid elements may be accelerated to higher or lower rapidities; these effects are complicated to predict, but we can state generally that they will always tend to *decrease* dE_T/dy where it has its maximum, namely, at $y = 0$. Given that we have strong evidence of thermalization and hydrodynamic evolution at RHIC collisions, it is likely that all these effects are present to some degree, and so we should suspect that final state $dE_T/d\eta$ is substantially lower than $dE_T(\tau_{\rm form})/dy$ at midrapidity.

Coming to the estimate of $\tau_{\rm form}$, the assumption that $\tau_{\rm form} = \hbar/\langle m_T \rangle$ cannot be taken as exact, even if the produced particles' m_T's are all identical, since "formed" is not an exact concept. However, if we accept the basic validity of this uncertainty principle argument, then we can see that the approximation in (35) provides a lower limit on $\langle m_T \rangle$. First, the numerator $dE_T/d\eta$ is a lower limit on $dE_T(\tau_{\rm form})/dy$, as above. Second, the argument is often made on grounds of entropy conservation that the local number density of particles can never decrease [98], which would make the final state denominator in (35) an upper limit on its early-time value.

Table 5: $E_T/N_{\rm ch}$ (GeV) as a function of $\sqrt{s_{\rm NN}}$, plotted in Figure 43.

$\sqrt{s_{\rm NN}}$ (GeV)	Coll. species	$E_T/N_{\rm ch}$ (GeV)	Reference
2.05	Au+Au	0.13 ± 0.03	[90]
3.81	Au+Au	0.598 ± 0.060	[83]
4.27	Au+Au	0.634 ± 0.063	[83]
4.84	Au+Au	0.680 ± 0.068	[83]
8.7	Pb+Pb	0.760 ± 0.060	[91, 92]
12.4	Pb+Pb	0.780 ± 0.060	[91, 92]
17.2	Pb+Pb	0.810 ± 0.060	[93]
19.6	Au+Au	0.738 ± 0.070	[83]
62.4	Au+Au	0.867 ± 0.121	[94, 95]
130	Au+Au	0.869 ± 0.066	[27]
200	Au+Au	0.881 ± 0.071	[83]
2760	Pb+Pb	1.283 ± 0.085	[28]

9. Transverse Energy per Charged Particle ($E_T/N_{\rm ch}$) and Freeze-Out Criteria

The ratio of pseudorapidity densities of transverse energy and number of charged particles at midrapidity, that is, $(dE_T/d\eta)/(dN_{\rm ch}/d\eta)(\equiv E_T/N_{\rm ch})$, has been studied both experimentally [28, 64, 83] and phenomenologically [99–104] to understand the underlying particle production mechanism. This observable is known as global barometric measure of the internal pressure in the ultradense matter produced in heavy-ion collisions. This quantity depends on the initial state of the collision and the viscosity of the matter as it expands to its final state, when it is observed by the detectors. This observable when studied as a function of collision energy (as shown in Figure 43 and the values are given in Table 5) shows three regions of interest. The first one from the lower SIS energies to SPS energies shows a steep increase of $E_T/N_{\rm ch}$ values, thereby indicating that the mean energy of the system increases (at midrapidity, $\langle E \rangle \sim \langle m_T \rangle$). In the second region, from SPS to top RHIC energy, $E_T/N_{\rm ch}$

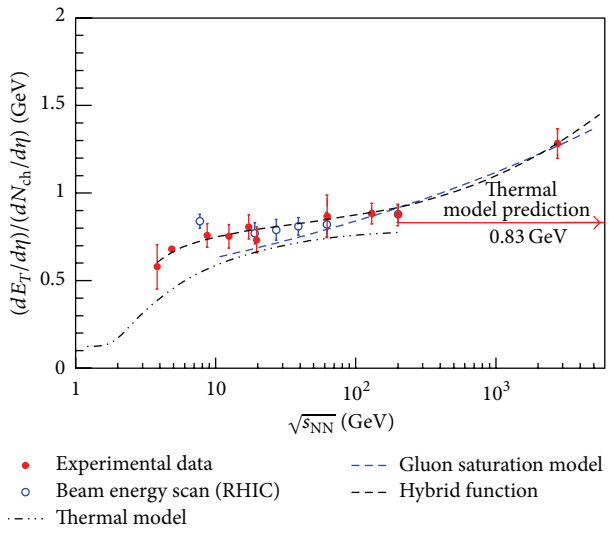

FIGURE 43: The ratio of $dE_T/d\eta$ and $dN_{ch}/d\eta$ at midrapidity, as a function of center of mass energy. Experimental data are compared to the predictions from thermal model, gluon saturation model, and the estimations obtained in the framework of the hybrid model fitting to transverse energy and charged particle data. The Figure is taken from [43].

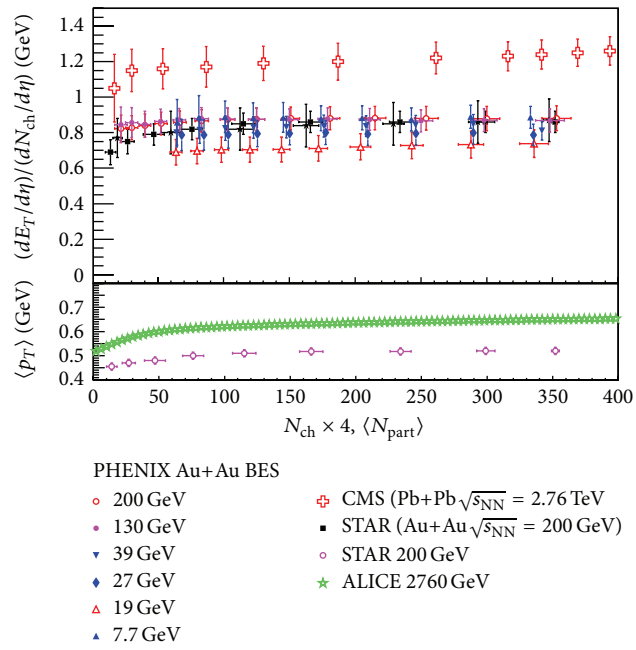

FIGURE 44: Upper panel: the midrapidity ($0 < \eta < 1$) E_T/N_{ch} as a function of collision centrality for a wide range of energies spanning RHIC beam energy scan to LHC. Lower panel: the mean transverse momentum as a function of collision centrality, for both top RHIC energy and LHC 2.76 TeV center of mass energy. A similar spectral behaviour is observed for $\langle p_T \rangle$ and the barometric observable, E_T/N_{ch}.

shows a very weak collision energy dependence, that is, like a saturation behaviour. In this region the mean energy does not increase, whereas the collision energy increases. This may indicate that the increase in collision energy results in new particle production in this energy domain, which is consistent with higher particle multiplicity observed at these energies. This behaviour has been well described in the context of a statistical hadron gas model (SHGM) [99, 100]. In the framework of SHGM, it has been predicted that E_T/N_{ch} would saturate at energies higher to that of top RHIC energy with a limiting value of 0.83 GeV [99, 100]. Here a static fireball is assumed at the freeze-out. However, a value of 1.25± 0.08 GeV is observed at the LHC 2.76 TeV center of mass energy recently, by the CMS collaboration [28]. This creates a third region in the excitation function of E_T/N_{ch}, showing a jump from top RHIC to LHC energies. In this region, along with particle multiplicity, the mean energy per particle also increases, which needs to be understood from theoretical models taking the dynamics of the time evolution of the created fireball. It is however observed that models based on final state gluon saturation (CGC like) seem to explain this behaviour in the excitation function of E_T/N_{ch} [43]. The RHIC Beam Energy Scan (BES) data seem to follow the overall trend of the collision energy dependence of E_T/N_{ch}. It has been seen in one of the previous works of one of us (Raghunath Sahoo) [100] that various freeze-out criteria like constant energy per particle ($\langle E \rangle/\langle N \rangle = 1.08$ GeV) [105], fixed baryon+antibaryon density ($n_B + n_{\overline{B}} \simeq 0.12$ fm^{-3}) [106], and fixed entropy density per T^3 ($s/T^3 \simeq 7$) [107, 108] seem to describe the qualitative energy dependent behaviour of E_T/N_{ch} quite consistently up to RHIC energies. As shown in the figure, a hybrid function which is a combination of logarithmic and power law in center of mass energy seems to describe the data quite well. At very high energies, the creation and annihilation of gluons balances out leading to gluon saturation. In the framework of gluon saturation models, the high energy behaviour of this observable is well described [43].

Figure 44 (upper panel) shows the centrality dependence of E_T/N_{ch} from $\sqrt{s_{NN}} = 7.7$ GeV to 2.76 TeV energy. These data are enlisted in Table 6. Since the centrality definitions by the CMS experiment for $dN_{ch}/d\eta$ and $dE_T/d\eta$ are different, fitting the centrality dependent $dN_{ch}/d\eta$ by a function, $(1/0.5N_{part})(dN_{ch}/d\eta) = AN_{part}^{\alpha}$, with $A = 2.63 \pm 0.24$ and $\alpha = 0.19 \pm 0.02$, we have evaluated the $dN_{ch}/d\eta$ values corresponding to the N_{part} values used to define the centrality classes for $dE_T/d\eta$. Then we have estimated the LHC values of E_T/N_{ch} at different centralities, which are given in Table 6 and are shown in Figure 44. Within the systematic errors, E_T/N_{ch} for all energies up to top RHIC energy show a weak centrality dependence with a modest increase from most peripheral collisions to $N_{part} = 100$, reaching a roughly constant value of around 0.8 GeV towards central collisions. The LHC data also show a similar behaviour but the constant value of E_T/N_{ch} is around 1.25 GeV. This centrality dependence of E_T/N_{ch} is shown to be equivalent to the behaviour of $\langle p_T \rangle$ as a function of centrality for top RHIC energy [64] and for $\sqrt{s_{NN}} = 2.76$ TeV [96] at LHC. This is shown in the lower panel of Figure 44. The value of $\langle p_T \rangle = 0.678 \pm 0.007$ GeV/c at $\sqrt{s_{NN}} = 2.76$ TeV, which is almost 36%

Table 6: E_T/N_{ch} (GeV) for different center of mass energies as a function of N_{part}, the measure of collision centrality (shown in Figure 44).

$\sqrt{s_{NN}}$ (GeV)	0–5	5–10	10–15	15–20	20–25	25–30	30–35	35–40	40–45	45–50	50–55	55–60	60–65	65–70
7.7	0.70	0.73	0.74	0.77	0.78	0.81	0.84	0.87	0.90	0.94				
19.6	1.07	1.11	1.14	1.17	1.18	1.22	1.24	1.27	1.30	1.36				
27	1.22	1.24	1.27	1.30	1.34	1.38	1.40	1.44	1.47	1.54				
39	1.41	1.45	1.47	1.51	1.54	1.58	1.61	1.66	1.71	1.69				
62.4	1.21	1.26	1.32	1.40	1.49	1.57	1.67	1.76	1.84	1.92	2.01	2.07	2.17	2.23
130	1.95	2.02	2.05	2.12	2.21	2.31	2.38	2.48	2.56	2.65	2.73	2.80	2.89	3.01
200	1.93	2.06	2.18	2.31	2.46	2.57	2.66	2.76	2.87	2.95	3.04	3.16	3.29	3.44
$\sqrt{s_{NN}}$ (TeV)	0–2.5	2.5–5	5–7.5	7.5–10	10–20	20–30	30–40	40–50	50–60	60–70	70–80			
2.76	1.26	1.25	1.24	1.23	1.22	1.21	1.19	1.17	1.16	1.15	1.05			

increase when compared with its value (~0.5 GeV/c) at top RHIC energy [64, 96]. The value of E_T/N_{ch} increases almost 45% from top RHIC to LHC energy. This shows that not only particle multiplicity increases while going from top RHIC to LHC energy, but the $\langle p_T \rangle$ also increases, making a third region in the excitation function of E_T/N_{ch}. The near centrality independent behaviour of E_T/N_{ch} is explained by statistical hadron gas model (SHGM) with a static fireball approximation at freeze-out [99]. However, to explain the energy dependent behaviour of E_T/N_{ch} in the whole range of energies up to LHC, one needs to consider the dynamical effects during the time evolution of fireball. Irrespective of the collisions species, the center of mass energies, and the collision centrality, starting from the lower energies to top RHIC energy, the system evolves to the same final state, which could be characterized by a constancy in chemical freeze-out temperature. On the other hand, LHC data shows a different trend of E_T/N_{ch}, while the chemical freeze-out temperature does not change that much from RHIC to LHC. This needs to be understood from the thermodynamics point of view [109, 110].

A theoretical description of the time evolution of the produced fireball in heavy-ion collisions is difficult, as it involves different degrees of freedoms at different points. The SHGM uses hadronic degrees of freedom at later times, when the chemical composition of the matter is frozen (known as chemical freeze-out). Then the particles mean free path becomes higher than the system size, which forbids the elastic collision of the constituents and the system is said to be kinetically frozen (known as thermal or kinetic freeze-out). In general, freeze-out could be a complicated process involving duration in time and a hierarchy, where different types of particles and reactions switch-off at different times. This leads to the concept of *"differential freeze-out."* From kinetic arguments, it is expected that reactions with lower cross sections switch off at higher densities/temperature compared to reactions with higher cross sections. Hence, the chemical freeze-out, which corresponds to inelastic reactions, occurs earlier in time compared to the kinetic freeze-out, which corresponds to elastic reactions. In accordance with the above discussions, one can think of strange or charmed particles decoupling from the system earlier than the lighter hadrons. A series of freeze-outs could be thought of corresponding to particular reaction channels [111]. However, in general one focuses on chemical and kinetic freeze-outs, considering the freeze-out to be an instantaneous process. At higher energies, when $\mu_B \sim 0$, the transverse energy production is mainly due to the meson content of the system. The experimental observations go in line with the above fact, when we observe the ratio of $\overline{p}/p \sim 1$ at higher energies [110]. The intersection points of lines of constant E_T/N_{ch} and the freeze-out line give the values of E_T/N_{ch} at the chemical freeze-out [99].

10. Summary and Conclusions

Pseudorapidity distribution of charged particles is proposed to be one of the important global observables to characterize the hot and dense medium produced in the heavy-ion collisions. We review the charged particle and photon multiplicity density distribution results obtained by various heavy-ion collision experiments starting from AGS energies to top RHIC and LHC energies. Before going to the results, a brief introduction on determination of centrality is given. Centrality determination is important in terms of relating theoretical observables, like impact parameters and numbers of nucleon participant (N_{part}), to the collision geometry and observed particle multiplicity. To correlate them, for example, two-component model with NBD is fitted with the V0 amplitude and the centrality percentile is evaluated to classify the events into different centralities. In the mean time the respective N_{part}, N_{coll} and impact parameters are estimated by Monte Carlo Glauber model. The $dN_{ch}/d\eta$ spectra are discussed for Cu+Cu, Au+Au, and Pb+Pb collisions at different energies. It is observed that the width and amplitude of the distribution increase with increase of collision energy. A double-Gaussian function is fitted with the distribution and it is found that the ratio of amplitudes and the widths are similar from one centrality to the other in their respective collision energy. More interestingly, the dip is observed to be higher in Pb+Pb collisions at $\sqrt{s_{NN}} = 2.76$ TeV at midrapidity. This is an indication of different hadro-chemistry at LHC energy compared to RHIC. In addition, this may be an interplay of the Jacobian and midrapidity gluonic and fragmentation sources contributing to particle production. Still this needs to be understood in detail. Similarly, the energy dependence of $dN_\gamma/d\eta$ of Cu+Cu, Au+Au, S+Au, and Pb+Pb collisions is discussed.

Then the limiting fragmentation behaviour of charged particles as well as photons is discussed for Cu+Cu, Au+Au, and Pb+Pb collisions at different energies. The compilation of various experimental data goes in line with the hypothesis of limiting fragmentation. Moreover, after observing the centrality dependence of longitudinal scaling of charged particles, R_{PC} is used to confirm the scaling behaviour and the scaling seems to be valid for a wide range of energies. In contrast to charged particles, photons do not show any centrality dependence. It is interpreted as majority of photons in the forward rapidities are coming from π^0 decays. Hence, mesons are not affected by baryon stopping as they are originated from valence quarks. CGC model has successfully explained the limiting fragmentation up to some extent. However, it needs more development and complete understanding of the final state effect and inclusion of quark distribution. This longitudinal scaling of hadrons still needs more insight to understand the physics process and its predicted violation at LHC energies in the frame work of SHGM and the validity from experimental data are to be understood from theoretical considerations.

During the discussion of factorization, it is also observed that the centrality dependence of $dN_{\mathrm{ch}}/d\eta$ can be factorized to beam energy and collision centrality. By taking the ratio of $dN_{\mathrm{ch}}/d\eta$ of Pb+Pb collision at $\sqrt{s_{\mathrm{NN}}} = 2.76\,\mathrm{TeV}$ to other collision energies, we observe a scaling behaviour as a function of N_{part}. To understand the expansion dynamics of the system, the $dN_{\mathrm{ch}}/d\eta$ of charged particles and photons are fitted with Landau-Carruthers and Gaussian functions. By taking the ratio of widths of data to the Landau-Carruthers function, it is found that the system is expanding more or less like a Landau hydrodynamic fluid up to the RHIC energy. But the LHC data deviate from the Landau hydrodynamic model, so far the shape of the pseudorapidity distribution is concerned. Similarly, photons at RHIC energies also obey the Landau hydrodynamics. It is observed that the $N_{\mathrm{ch}}^{\mathrm{total}}$ normalized to N_{part} scales with centrality. It is to be noted here that in the midrapidity $dN_{\mathrm{ch}}/d\eta$ normalized to N_{part} does not scale with centrality, whereas the total charged particles do. This is because, the modification of charged particles at forward rapidities is strongly correlated with compensating changes at midrapidity. $dN_{\gamma}/d\eta$ also shows similar scaling. It is found that trapezoidal rule can be used to explain the $N_{\mathrm{ch}}^{\mathrm{total}}$ normalized to participant pair from AGS energies to RHIC energies. However, it fails at LHC energy. A hybrid function, which is a combination of power-law and logarithmic in $\sqrt{s_{\mathrm{NN}}}$, seems to explain the whole range of data indicating that the charged particle production is a combined process of midrapidity gluonic sources (power law) and fragmentation sources (logarithmic).

The transverse energy measurement and the estimation of initial energy density in the framework of Bjorken boost invariant hydrodynamics are presented for collision energies ranging from few GeV to TeV. In this energy domain, the centrality and energy dependence of $dE_T/d\eta$ and Bjorken energy density multiplied with formation time $\epsilon_{\mathrm{Bj}} \cdot \tau$ have been studied. A comparison of ϵ_{Bj} with that of lQCD value indicates the formation of a QGP phase both at RHIC and at LHC energies. The barometric observable, that is, transverse energy per charged particle, is related to the chemical freeze-out. Various freeze-out criteria seem to describe the energy dependent behaviour of E_T/N_{ch} starting from few GeV to top RHIC energies. A static fireball approximation at freeze-out, however, fails to reproduce the corresponding data at LHC and necessitates the inclusion of fireball evolution dynamics in space and time in order to describe the behaviour for the whole range of energies. The similarity in the centrality dependence up to the top RHIC energy indicates that irrespective of the collision species and center of mass energies, the system evolves to a similar final state at freeze-out.

Note. In this review, we have made an attempt to give the developments in heavy-ion collisions towards the measurements of charged particle and photon multiplicities along with transverse energy production from few GeV to TeV energies. Although we have tried to cover it in some detail, it is not an easy task and we can never assume the task to be complete. However, we believe that the references mentioned in this review will guide the readers in the related fields. We apologize to those authors whose valuable contributions in this area have not been mentioned properly.

Appendix

The Gamma and Negative Binomial Distributions

The Gamma distribution represents the probability density for a continuous variable x and has two parameters b and p. This is given by

$$f(x) = f_{\Gamma}(x, p, b) = \frac{b}{\Gamma(p)} (bx)^{p-1} e^{-bx}, \tag{A.1}$$

where

$$p > 0, \quad b > 0, \quad 0 \le x \le \infty. \tag{A.2}$$

$\Gamma(p) = (p-1)!$ is the Gamma function if p is an integer, and $f(x)$ is normalized, $\int_0^{\infty} f(x)dx = 1$. The first few moments of the distribution are

$$\mu \equiv \langle x \rangle = \frac{p}{b}, \qquad \sigma \equiv \sqrt{\langle x^2 \rangle - \langle x \rangle^2} = \frac{\sqrt{p}}{b}, \qquad \frac{\sigma^2}{\mu^2} = \frac{1}{p}. \tag{A.3}$$

The Negative Binomial Distribution (NBD) of an integer m is defined as

$$P(m) = \frac{(m+k-1)!}{m!\,(k-1)!} \frac{(\mu/k)^m}{(1+\mu/k)^{m+k}}, \tag{A.4}$$

where $P(m)$ is normalized for $0 \le m \le \infty$, $\mu \equiv \langle m \rangle$, and some of the higher moments are

$$\sigma = \sqrt{\mu\left(1 + \frac{\mu}{k}\right)}, \qquad \frac{\sigma^2}{\mu^2} = \frac{1}{\mu} + \frac{1}{k}. \tag{A.5}$$

The NBD is having an additional parameter k compared to a Poisson distribution. In the limit $k \to \infty$ NBD becomes a Poissonian distribution. With k equals to a negative integer (hence the name), it becomes a NBD. The NBD is strongly correlated with Gamma distribution and hence becomes Gamma distribution in the limit $\mu \gg k > 1$. Usually Gamma distributions are replaced with NBD to prove various theorems [112]. One important difference between NBD and Gamma distributions is in the limit m or $x \to 0$: for $p > 1$ the limit is always zero for a Gamma distribution, whereas for the NBD it is always finite. A detailed discussion on different probability distributions could be found in [113, 114].

The Gamma distribution has got potential applications as under *convolution* it shows an important property. Define the n-fold convolution of a distribution with itself as

$$f_n(x) = \int_0^x dy f(y) f_{n-1}(x-y); \tag{A.6}$$

then for a Gamma distribution given by (A.1), the n-fold convolution is simply given by the function

$$f_n(x) = \frac{b}{\Gamma(np)} (bx)^{np-1} e^{-bx} = f_\Gamma(x, np, b); \tag{A.7}$$

that is, $p \to np$ and b remains unchanged. Note that the mean μ_n and the standard deviation σ_n of the n-fold convolution obey the familiar rule

$$\mu_n = n\mu = \frac{np}{b}, \qquad \sigma_n = \sigma\sqrt{n} = \frac{\sqrt{np}}{b}, \qquad \frac{\sigma_n}{\mu_n} = \frac{1}{\sqrt{np}}. \tag{A.8}$$

The convolution property of the Gamma distribution also holds good for the NBD, with $\mu_n \to n\mu$, $k \to nk$, so that μ/k remains constant [78]. Note that the charged particle multiplicity distribution in proton-proton collisions obeys NBD [18, 20], whereas the Gamma distribution fits to E_T distributions [115, 116].

Conflict of Interests

The authors declare that there is no conflict of interests regarding the publication of this paper.

Acknowledgments

The authors would like to thank Dr. Edward K. G. Sarkisyan for useful discussions and careful reading of this review. Dr. Prabhat Pujahari is acknowledged for useful discussions. Ms. Pooja Pareek is acknowledged for her help in replotting some of the figures.

References

[1] J. C. Collins and M. J. Perry, "Superdense matter: neutrons or asymptotically free quarks?" *Physical Review Letters*, vol. 34, no. 21, pp. 1353–1356, 1975.

[2] J. D. Bjorken, "Highly relativistic nucleus-nucleus collisions: the central rapidity region," *Physical Review D*, vol. 27, no. 1, pp. 140–151, 1983.

[3] F. Karsch, "Lattice results on QCD thermodynamics," *Nuclear Physics A*, vol. 698, no. 1–4, pp. 199–208, 2002.

[4] M. Kataja, P. V. Ruuskanen, L. D. McLerran, and H. von Gersdorff, "Studies of the hydrodynamic evolution of matter produced in fluctuations in $p\bar{p}$ collisions and in ultrarelativistic nuclear collisions. II. Transverse-momentum distributions," *Physical Review D*, vol. 34, p. 2755, 1986.

[5] L. van Hove, "Multiplicity dependence of p_t spectrum as a possible signal for a phase transition in hadronic collisions," *Physics Letters B*, vol. 118, no. 1–3, pp. 138–140, 1982.

[6] S. Sarkar, D. K. Srivastava, and B. Sinha, "Rapidity distribution of photons emitted from a hadronizing quark-gluon plasma," *Physical Review C*, vol. 51, no. 1, pp. 318–327, 1995, Erratum in *Physical Review C*, vol. 51, p. 2845, 1995.

[7] A. Dumitru, U. Katscher, J. A. Maruhn, H. Stöcker, W. Greiner, and D. H. Rischke, "Thermal photons as a measure for the rapidity dependence of the temperature," *Zeitschrift für Physik A*, vol. 353, no. 2, pp. 187–190, 1995.

[8] D. Kharzeev and M. Nardi, "Hadron production in nuclear collisions at RHIC and high-density QCD," *Physics Letters B*, vol. 507, no. 1–4, pp. 121–128, 2001.

[9] B. B. Back, M. D. Baker, M. Ballintijn et al., "Charged-particle pseudorapidity distributions in Au+Au collisions at $\sqrt{s_{NN}}$ = 62.4 GeV," *Physical Review C*, vol. 74, Article ID 021901, 2006.

[10] M. C. Abreu, B. Alessandro, C. Alexa et al., "Scaling of charged particle multiplicity in Pb-Pb collisions at SPS energies," *Physics Letters B*, vol. 530, pp. 43–55, 2002.

[11] E. Abbas, B. Abelev, J. Adam et al., "Centrality dependence of the pseudorapidity density distribution for charged particles in Pb–Pb collisions at $\sqrt{s_{NN}}$ = 2.76TeV," *Physics Letters B*, vol. 726, no. 4-5, pp. 610–622, 2013.

[12] B. B. Back, M. D. Baker, M. Ballintijn et al., "Collision geometry scaling of Au + Au pseudorapidity density from $\sqrt{s_{NN}}$ = 19.6 to 200 GeV," *Physical Review C*, vol. 70, Article ID 021902(R), 2004.

[13] B. Alver, B. B. Back, M. D. Baker et al., "Charged-particle multiplicity and pseudorapidity distributions measured with the PHOBOS detector in Au+Au, Cu+Cu, d+Au, and p+p collisions at ultrarelativistic energies," *Physical Review C*, vol. 83, no. 2, Article ID 024913, 24 pages, 2011.

[14] G. Aad, B. Abbott, J. Abdallah et al., "Measurement of the centrality dependence of the charged particle pseudorapidity distribution in lead-lead collisions at $\sqrt{s_{NN}}$ = 2.76 Tev with the ATLAS detector," *Physics Letters B*, vol. 710, pp. 363–382, 2012.

[15] S. Chatrchyan, V. Khachatryan, A. M. Sirunyan et al., "Dependence on pseudorapidity and on centrality of charged hadron production in PbPb collisions at $\sqrt{S_{NN}}$ = 2.76 TeV," *Journal of High Energy Physics*, vol. 8, p. 141, 2011.

[16] B. Abelev, J. Adam, D. Adamová et al., "Centrality determination of Pb-Pb collisions at $\sqrt{s_{NN}}$ = 2.76 TeV with ALICE," *Physical Review C*, vol. 88, Article ID 044909, 2013.

[17] B. Abelev, J. Adam, D. Adamová et al., "Measurement of the cross section for electromagnetic dissociation with neutron emission in Pb-Pb collisions at $\sqrt{s_{\mathrm{NN}}}$ = 2.76 TeV," *Physical Review Letters*, vol. 109, Article ID 252302, 2012.

[18] W. Kittel and E. A. De Wolf, *Soft Multihadron Dynamics*, World Scientific, New York, NY, USA, 2005.

[19] I. M. Dremin and J. W. Gary, "Hadron multiplicities," *Physics Report*, vol. 349, no. 4, pp. 301–393, 2001.

[20] J. F. Grosse-Oetringhaus and K. Reygers, "Charged-particle multiplicity in proton-proton collisions," *Journal of Physics G: Nuclear and Particle Physics*, vol. 37, no. 8, Article ID 083001, 2010.

[21] K. Aamodt, A. Abrahantes Quintana, D. Adamová et al., "Centrality dependence of the charged-particle multiplicity density at midrapidity in Pb-Pb collisions at $\sqrt{s_{\mathrm{NN}}} = 2.76$ TeV," *Physical Review Letters*, vol. 106, Article ID 032301, 2011.

[22] B. Alver, B. B. Back, M. D. Baker et al., "System size, energy, and centrality dependence of pseudorapidity distributions of charged particles in relativistic heavy-ion collisions," *Physical Review Letters*, vol. 102, Article ID 142301, 2009.

[23] B. B. Back, M. D. Baker, D. S. Barton et al., "Significance of the fragmentation region in ultrarelativistic heavy-ion collisions," *Physical Review Letters*, vol. 91, Article ID 052303, 2003.

[24] P. Carruthers and M. Duong-van, "Rapidity and angular distributions of charged secondaries according to the hydrodynamical model of particle production," *Physical Review D*, vol. 8, no. 3, pp. 859–874, 1973.

[25] F.-H. Liu, Y.-H. Chen, Y.-Q. Gao, and E.-Q. Wang, "On current conversion between particle rapidity and pseudorapidity distributions in high energy collisions," *Advances in High Energy Physics*, vol. 2013, Article ID 710534, 4 pages, 2013.

[26] C. Y. Wong, *Introduction to High Energy Heavy-Ion Collisions*, World Scientific, River Edge, NJ, USA, 1994.

[27] K. Adcox, S. S. Adler, N. N. Ajitanand et al., "Measurement of the midrapidity transverse energy distribution from $\sqrt{s_{\mathrm{NN}}} = 130$ GeV Au + Au collisions at RHIC," *Physical Review Letters*, vol. 87, Article ID 052301, 2001.

[28] S. Chatrchyan, V. Khachatryan, A. M. Sirunyan et al., "Measurement of the pseudorapidity and centrality dependence of the transverse energy density in Pb-Pb collisions at $\sqrt{s_{NN}} = 2.76$ TeV," *Physical Review Letters*, vol. 109, Article ID 152303, 2012.

[29] G. Wolschin, "Particle production sources at LHC energies," *Journal of Physics G*, vol. 40, no. 4, Article ID 045104, 2013.

[30] L. D. Landau, "On the multiparticle production in high-energy collisions," *Izvestiya Akademii Nauk SSR, Seriya Fizicheskaya*, vol. 17, pp. 51–64, 1953.

[31] C. Alt, T. Anticic, B. Baatar et al., "Pion and kaon production in central Pb + Pb collisions at 20*A* and 30*A* GeV: evidence for the onset of deconfinement," *Physical Review C*, vol. 77, Article ID 024903, 2008.

[32] H. Petersen and M. Bleicher, "Longitudinal flow and onset of deconfinement," in *Proceedings of the 3rd International Workshop The Critical Point and Onset of Deconfinement*, Firenze, Italy, 2006.

[33] B. Mohanty and J. Alam, "Velocity of sound in relativistic heavy-ion collisions," *Physical Review C*, vol. 68, Article ID 064903, 2003.

[34] J. Benecke, T. T. Chou, C. N. Yang, and E. Yen, "Hypothesis of limiting fragmentation in high-energy collisions," *Physical Review*, vol. 188, no. 5, pp. 2159–2169, 1969.

[35] G. J. Alner, R. E. Ansorge, B. Åsman et al., "Scaling of pseudorapidity distributions at c.m. energies up to 0.9 TeV," *Zeitschrift für Physik C*, vol. 33, no. 1, pp. 1–6, 1986.

[36] B. B. Back, M. D. Baker, M. Ballintijn et al., "Scaling of charged particle production in d + Au collisions at $\sqrt{s_{\mathrm{NN}}} = 200$ GeV," *Physical Review C*, vol. 72, Article ID 031901, 2005.

[37] B. B. Back, M. D. Baker, D. S. Barton et al., "Centrality and energy dependence of charged-particle multiplicities in heavy ion collisions in the context of elementary reactions," *Physical Review C*, vol. 74, no. 2, Article ID 021902, 4 pages, 2006.

[38] G. Antchev, P. Aspell, I. Atanassov et al., "Luminosity-independent measurements of total, elastic and inelastic cross-sections at $\sqrt{s} = 7$ TeV," *Europhysics Letters*, vol. 101, no. 2, Article ID 21004, 2013.

[39] J. Jalilian-Marian, "Limiting fragmentation from the color glass condensate," *Physical Review C*, vol. 70, no. 2, Article ID 027902, 3 pages, 2004.

[40] F. Gelis, A. M. Staśto, and R. Venugopalan, "Limiting fragmentation in hadron–hadron collisions at high energies," *The European Physical Journal C*, vol. 48, no. 2, pp. 489–500, 2006.

[41] J. Cleymans, J. Strümpfer, and L. Turko, "Extended longitudinal scaling and the thermal model," *Physical Review C*, vol. 78, no. 1, Article ID 017901, 2008.

[42] P. Brogueira, J. D. D. Deus, and C. Pajares, "Limiting fragmentation in heavy-ion collisions and percolation of strings," *Physical Review C*, vol. 75, no. 5, Article ID 054908, 2007.

[43] R. Sahoo and A. N. Mishra, "Transverse energy and charged particle production in heavy-ion collisions: from RHIC to LHC," *International Journal of Modern Physics E*, vol. 23, no. 4, Article ID 1450024, 2014.

[44] A. Biallas, M. Bleszynski, and W. Czyz, "Multiplicity distributions in nucleus-nucleus collisions at high energies," *Nuclear Physics B*, vol. 111, pp. 461–476, 1976.

[45] X.-N. Wang and M. Gyulassy, "Energy and centrality dependence of rapidity densities at RHIC energies," *Physical Review Letters*, vol. 86, no. 16, article 3496, 2001.

[46] P. Steinberg, "Entropy production at high energy and μ_B," *Proceedings of Science CPOD*, vol. 2006, article 036, 2006.

[47] E. K. G. Sarkisyan and A. S. Sakharov, "Multihadron production features in different reactions," *AIP Conference Proceedings*, vol. 828, no. 1, pp. 35–41, 2006.

[48] C. Y. Wong, "Landau hydrodynamics reexamined," *Physical Review C*, vol. 78, Article ID 054902, 2008.

[49] P. K. Netrakanti and B. Mohanty, "Width of the rapidity distribution in heavy-ion collisions," *Physical Review C*, vol. 71, Article ID 047901, 2005.

[50] P. Carruthers and M. Doung-van, "New scaling law based on the hydrodynamical model of particle production," *Physics Letters B*, vol. 41, no. 5, pp. 597–601, 1972.

[51] G. Wolschin, "Relativistic diffusion model," *The European Physical Journal A*, vol. 5, no. 1, pp. 85–90, 1999.

[52] P. Tribedy and R. Venugopalan, "QCD saturation at the LHC: comparisons of models to p + p and A + A data and predictions for p + Pb collisions," *Physics Letters B*, vol. 710, no. 1, pp. 125–133, 2012.

[53] A. N. Mishra, R. Sahoo, E. K. G. Sarkisyan, and A. S. Sakharov, "Effective-energy budget in multiparticle production in nuclear collisions," *The European Physical Journal C*, vol. 74, article 3147, 2014.

[54] S. Eremin and S. Voloshin, "Nucleon participants or quark participants?" *Physical Review C*, vol. 67, Article ID 064905, 2003.

[55] P. K. Netrakanti and B. Mohanty, "Quark participants and global observables," *Physical Review C*, vol. 70, Article ID 027901, 2004.

[56] B. De and S. Bhattacharyya, "Rapidity spectra of the secondaries produced in heavy ion collisions and the constituent picture of the particles," *Physical Review C*, vol. 71, Article ID 024903, 2005.

[57] R. Nouicer, "Similarity of initial states in A+A and p+p collisions in constituent quarks framework," *AIP Conference Proceedings*, vol. 828, p. 11, 2006.

[58] R. Nouicer and PHOBOS Collaboration, "Systematics of global observables in Cu+Cu and Au+Au collisions at RHIC energies," *AIP Conference Proceedings*, vol. 842, p. 86, 2006.

[59] R. Nouicer, "Charged particle multiplicities in A+A and p+p collisions in the constituent quarks framework," *The European Physical Journal C*, vol. 49, no. 1, pp. 281–286, 2007.

[60] E. K. G. Sarkisyan and A. S. Sakharov, "Relating multihadron production in hadronic and nuclear collisions," *European Physical Journal C*, vol. 70, no. 3, pp. 533–541, 2010.

[61] J. D. Bjorken, "A full-acceptance detector for SSC physics at low and intermediate mass scales: an expression of interest to the SSC," *International Journal of Modern Physics A*, vol. 7, no. 18, p. 4189, 1992.

[62] J. D. Bjorken, K. L. Kowalski, and C. C. Taylor, "Baked Alaska," Tech. Rep. SLAC-PUB-6109, 1993.

[63] K. Rajagopal and F. Wilczek, "Static and dynamic critical phenomena at a second order QCD phase transition," *Nuclear Physics B*, vol. 399, no. 2-3, pp. 395–425, 1993.

[64] J. Adams, M. M. Aggarwal, Z. Ahammed et al., "Measurements of transverse energy distributions in Au+Au collisions at $\sqrt{s_{NN}}$=200 GeV," *Physical Review C*, vol. 70, Article ID 054907, 2004.

[65] B. I. Abelev, M. M. Aggarwal, Z. Ahammed et al., "Center of mass energy and system-size dependence of photon production at forward rapidity at RHIC," *Nuclear Physics A*, vol. 832, no. 1-2, pp. 134–147, 2010.

[66] J. Adams, M. M. Aggarwal, Z. Ahammed et al., "Multiplicity and pseudorapidity distributions of photons in Au+Au collisions at $\sqrt{s_{NN}}$ = 62.4 GeV," *Physical Review Letters*, vol. 95, Article ID 062301, 2005.

[67] M. M. Aggarwal, A. L. S. Angelis, V. Antonenko et al., "Multiplicity and pseudorapidity distribution of photons in S + Au reaction at 200*A* GeV," *Physical Review C*, vol. 58, pp. 1146–1154, 1998.

[68] M. M. Aggarwal, A. Agnihotri, Z. Ahammed et al., "Systematics of inclusive photon production in 158-A-GeV Pb induced reactions on Ni, Nb, and Pb targets," *Physics Letters B*, vol. 458, pp. 422–430, 1999.

[69] M. Jacob and P. V. Landshoff, "Minijets: origin and usefulness," *Modern Physics Letters A*, vol. 1, no. 12, article 657, 1986.

[70] X. N. Wang, "A pQCD-based approach to parton production and equilibration in high-energy nuclear collisions," *Physics Reports*, vol. 280, no. 5-6, pp. 287–371, 1997.

[71] M. Gyulassy and T. Matsui, "Quark-gluon-plasma evolution in scaling hydrodynamics," *Physical Review D*, vol. 29, no. 3, pp. 419–425, 1984.

[72] K. J. Eskola, K. Kajantie, P. V. Ruuskanen, and K. Tuominen, "Scaling of transverse energies and multiplicities with atomic number and energy in ultrarelativistic nuclear collisions," *Nuclear Physics B*, vol. 570, no. 1-2, pp. 379–389, 2000.

[73] P. F. Kolb, U. Heinz, P. Huovinen, K. J. Eskola, and K. Tuominen, "Centrality dependence of multiplicity, transverse energy, and elliptic flow from hydrodynamics," *Nuclear Physics A*, vol. 696, no. 1-2, pp. 197–215, 2001.

[74] A. Dumitru and M. Gyulassy, "The effective pressure of a saturated gluon plasma," *Physics Letters, Section B: Nuclear, Elementary Particle and High-Energy Physics*, vol. 494, no. 3-4, pp. 215–220, 2000.

[75] T. Abbott, L. Ahle, Y. Akiba et al., "Systematics of midrapidity transverse energy distributions in limited apertures from p + Be to Au+Au," *Physical Review C*, vol. 63, Article ID 064602, 2001.

[76] K. Adcox, S. S. Adler, S. Afanasiev et al., "Formation of dense partonic matter in relativistic nucleus–nucleus collisions at RHIC: experimental evaluation by the PHENIX collaboration," *Nuclear Physics A*, vol. 757, no. 1-2, pp. 184–283, 2005.

[77] E. A. de Wolf, "Intermittency, negative binomials and two particle correlations," *Acta Physica Polonica B*, vol. 21, no. 8, pp. 611–626, 1990.

[78] T. Abbott, Y. Akiba, D. Alburger et al., "Multiplicity distributions from central collisions of ^{16}O+Cu at 14.6A GeV/c and intermittency," *Physical Review C*, vol. 52, article 2663, 1995.

[79] P. Ghosh, "Negative binomial multiplicity distribution in proton-proton collisions in limited pseudorapidity intervals at LHC up to $\sqrt{s}$ = 7 TeV and the clan model," *Physical Review D*, vol. 85, Article ID 054017, 2012.

[80] L. Ahle, Y. Akiba, K. Ashktorab et al., "Simultaneous multiplicity and forward energy characterization of particle spectra in Au + Au collisions at 11.6*A* GeV/c," *Physical Review C*, vol. 59, no. 4, p. 2173, 1999.

[81] F. Karsch, "Lattice results on QCD at high temperature and nonzero baryon number density," *Progress in Particle and Nuclear Physics*, vol. 62, pp. 503–511, 2009.

[82] Z. Fodor and S. D. Katz, "Critical point of QCD at finite T and μ, lattice results for physical quark masses," *Journal of High Energy Physics*, vol. 4, article 050, 2004.

[83] S. S. Adler, S. Afanasiev, C. Aidala et al., "Systematic studies of the centrality and $\sqrt{s_{NN}}$ dependence of the $dE_T/d\eta$ and $dN_{\mathrm{ch}}/d\eta$," *Physical Review C*, vol. 71, Article ID 034908, 2005.

[84] B. Hahn, D. G. Ravenhall, and R. Hofstadter, "High-energy electron scattering and the charge distributions of selected nuclei," *Physical Review*, vol. 101, pp. 1131–1142, 1956.

[85] C. W. de Jager, H. de Vries, and C. de Vries, "Nuclear charge and magnetization density distribution parameters from elastic electron scattering," *Atomic Data and Nuclear Data Tables*, vol. 14, no. 5-6, pp. 479–508, 1974.

[86] T. Alber, H. Appelshäuser, J. Bächler et al., "Transverse energy production in ^{208}Pb + Pb collisions at 158 GeV per nucleon," *Physical Review Letters*, vol. 75, no. 21, pp. 3814–3817, 1995.

[87] T. S. Ullrich, "Experimental summary on global observables, hadron spectra and ratios," *Nuclear Physics A*, vol. 715, pp. 399c–411c, 2003.

[88] J. Adams, C. Adler, M. M. Aggarwal et al., "Particle-type dependence of azimuthal anisotropy and nuclear modification of particle production in Au + Au collisions at $\sqrt{s_{\mathrm{NN}}}$ = 200 GeV," *Physical Review Letters*, vol. 92, Article ID 052302, 2004.

[89] P. F. Kolb and U. Heinz, "Hydrodynamic description of ultrarelativistic heavy-ion collisions," http://arxiv.org/abs/nucl-th/0305084.

[90] W. Reisdorf, "Central collisions of Au on Au at 150, 250 and 400 *A*·MeV," *Nuclear Physics A*, vol. 612, no. 3-4, pp. 493–556, 1997.

[91] M. van Leeuwen, S. V. Afanasiev, T. Anticic et al., "Recent results on spectra and yields from NA49," *Nuclear Physics A*, vol. 715, pp. 161c–170c, 2003.

[92] S. V. Afanasiev, T. Anticic, D. Barna et al., "Energy dependence of pion and kaon production in central Pb + Pb collisions," *Physical Review C*, vol. 66, Article ID 054902, 2002.

[93] F. Siklér, J. Bächler, D. Barna et al., "Hadron production in nuclear collisions from the NA49 experiment at 158 GeV/$c \cdot A$," *Nuclear Physics A*, vol. 661, no. 1–4, pp. 45–54, 1999.

[94] R. Sahoo, *Transverse energy measurement and fluctuation studies in ultra-relativistic heavy ion collisions [Ph.D. thesis]*, Utkal University, Bhubaneswar, India, 2007.

[95] R. Sahoo and STAR Collaboration, "Transverse energy measurement in Au+Au collisions by the STAR experiment," *Indian Journal of Physics*, vol. 85, no. 6, pp. 897–901, 2011.

[96] B. Abelev, J. Adamal, D. Adamová et al., "Multiplicity dependence of the average transverse momentum in pp, p-Pb, and Pb-Pb collisions at the LHC," *Physics Letters B*, vol. 727, no. 4-5, pp. 371–380, 2013.

[97] C. Markert, R. Bellwied, and I. Vitev, "Formation and decay of hadronic resonances in the QGP," *Physics Letters B*, vol. 669, no. 1, pp. 92–97, 2008.

[98] A. Krasnitz, Y. Nara, and R. Venugopalan, "Gluon production in the Color Glass Condensate model of collisions of ultrarelavistic finite nuclei," *Nuclear Physics A*, vol. 717, no. 3-4, pp. 268–290, 2003.

[99] J. Cleymans, R. Sahoo, D. P. Mahapatra, D. K. Srivastava, and S. Wheaton, "Transverse energy per charged particle and freeze-out criteria in heavy-ion collisions," *Physics Letters, Section B: Nuclear, Elementary Particle and High-Energy Physics*, vol. 660, no. 3, pp. 172–175, 2008.

[100] J. Cleymans, R. Sahoo, D. P. Mahapatra, D. K. Srivastava, and S. Wheaton, "Saturation of E_T/N_{ch} and freeze-out criteria in heavy-ion collisions," *Journal of Physics G*, vol. 35, no. 10, Article ID 104147, 2008.

[101] D. Prorok, "The transverse energy per charged particle estimates in the framework of a statistical model," *Nuclear Physics A*, vol. 749, pp. 194–197, 2005.

[102] D. Prorok, "The centrality dependence of transverse-energy and charged-particle multiplicity at RHIC: statistical model analysis," *The European Physical Journal A—Hadrons and Nuclei*, vol. 26, no. 2, pp. 277–284, 2005.

[103] D. Prorok, "Centrality dependence of global variables in relativistic heavy ion collisions: final pT data analysis in the framework of a statistical model," *Physical Review C*, vol. 73, Article ID 064901, 2006.

[104] D. Prorok, "Statistical hadronization model approach to $\sqrt{s_{NN}}$ = 200 GeV Au-Au collisions: p_T-spectra fits and global variable predictions," *Physical Review C*, vol. 75, Article ID 014903, 2007.

[105] J. Cleymans and K. Redlich, "Unified description of freeze-out parameters in relativistic heavy ion collisions," *Physical Review Letters*, vol. 81, no. 24, pp. 5284–5286, 1998.

[106] P. Braun-Munzinger and J. Stachel, "Particle ratios, equilibration and the QCD phase boundary," *Journal of Physics G: Nuclear and Particle Physics*, vol. 28, no. 7, pp. 1971–1976, 2002.

[107] A. Tawfik, "Influence of strange quarks on the QCD phase diagram and chemical freeze-out," *Journal of Physics G*, vol. 31, no. 6, Article ID S1105, 2005.

[108] J. Cleymans, H. Oeschler, K. Redlich, and S. Wheaton, "Transition from baryonic to mesonic freeze-out," *Physics Letters B*, vol. 615, no. 1-2, pp. 50–54, 2005.

[109] A. Adronic, P. Braun-Munzinger, J. Stachel, and H. Stocker, "Production of light nuclei, hypernuclei and their antiparticles in relativistic nuclear collisions," *Physics Letters B*, vol. 697, no. 3, pp. 203–207, 2011.

[110] B. Abelev, J. Adam, D. Adamová et al., "Pion, kaon, and proton production in central Pb-Pb collisions at $\sqrt{s_{\mathrm{NN}}}$ = 2.76 TeV," *Physical Review Letters*, vol. 109, Article ID 252301, 2012.

[111] A. Baran, W. Broniowski, and W. Florkowski, "Description of the particle ratios and transverse-momentum spectra for various centralities at RHIC in a single-freeze-out model," *Acta Physica Polonica B*, vol. 35, pp. 779–798, 2004.

[112] A. Bialas and R. Peschanski, "Random cascading models and the link between long-range and short-range interactions in multiparticle production," *Physics Letters B*, vol. 207, no. 1, pp. 59–63, 1988.

[113] A. Stuart and K. Ord, *Kendall's Advances Theory of Statistics*, vol. 1, Oxford University Press, Oxford, UK, 6th edition, 1994.

[114] W. Feller, *An Introduction to Probability: Theory and Its Applications*, vol. 1, John Wiley & Sons, New York, NY, USA, 3rd edition, 2008.

[115] M. J. Tannenbaum, "E_T and other event-by-event distributions from AGS to RHIC energies," *Progress in Particle and Nuclear Physics*, vol. 53, no. 1, pp. 239–252, 2004.

[116] J. Rak and M. J. Tannenbaum, *High pT Physics in the Heavy Ion Era*, Cambridge University Press, Cambridge, UK, 1st edition, 2013.